https://doi.org/10.5194/egusphere-2022-854
Preprint. Discussion started: 27 September 2022

OH measurements in the coastal atmosphere of South China: missing OH sinks in aged air masses

Zhouxing Zou[1], Qianjie Chen[1], Men Xia[1], Qi Yuan[1], Yi Chen[2], Yanan Wang[1], Enyu Xiong[1], Zhe Wang[2], and Tao Wang[1*]

[1]Department of Civil and Environmental Engineering, The Hong Kong Polytechnic University, Hong Kong, China

[2]Division of Environment and Sustainability, The Hong Kong University of Science and Technology, Hong Kong, China

Correspondence to:

Tao Wang (tao.wang@polyu.edu.hk)

Abstract

The hydroxyl radical (OH) is the main oxidant responsible for the removal of many reduced trace gases and the formation of secondary air pollutants. However, due to technical difficulties in measuring OH, the existing measurements of atmospheric OH concentrations are limited, and its sources and sinks are not well understood under low NO_x conditions. In this study, we observed the OH concentrations using chemical ionization mass spectrometry at a coastal site in Hong Kong from October to November 2020. The average noontime OH concentration over the study period was measured at $4.9 \pm 2.1 \times 10^6$ cm^{-3}. We found that a box model with comprehensive observational constraints reproduced the observed daytime OH concentrations when air parcels originated from the continental regions. However, this model overpredicted the observed daytime OH concentrations for coastal air parcels by 73% on average. Missing OH reactivity is proposed to be the cause of this overprediction. High missing OH reactivity was found in the case of low concentrations of nitrogen oxides (NO_x) and volatile organic compounds, as well as in aged air, suggesting that there could be unmeasured chemical species that cause the model to overestimate OH in aged coastal air parcels. Further studies are needed to identify these unmeasured chemical species and their contributions to the OH budget, in order to better quantify the formation of

https://doi.org/10.5194/egusphere-2022-854
Preprint. Discussion started: 27 September 2022

secondary air pollutants.

1. Introduction

The hydroxyl radical (OH) dominate atmospheric oxidative capacity and participates in nearly all sunlit tropospheric chemistry. The primary sources of the ambient OH radical include the photolysis of ozone (O_3) and nitrous acid (HONO) and the ozonolysis of alkenes. OH sinks are mainly the reactions of OH with trace gases, including carbon monoxide (CO), sulfur dioxide (SO_2), nitric oxide (NO), nitrogen dioxide (NO_2), methane, and other volatile organic compounds (VOCs; Fuchs et al., 2018). Heterogeneous uptake of OH represents very minor OH sinks (Ivanov et al., 1996). In reactions with CO and VOCs, peroxy radicals (HO_2 and RO_2) are produced and then recycled back into OH in the presence of NO as a secondary OH source. This interconversion is closely related to photochemical smog production (Stone et al., 2012). The reaction of OH with SO_2 and NO_2 produces H_2SO_4 and HNO_3, contributing to new particle formation and the acidity of rain, fog, and aerosols. OH also plays an important role in the climate system through reactions with the greenhouse gas CH_4 and the sulfate aerosol precursor dimethyl sulfide (DMS)(Berresheim, 2002).

Measuring ambient OH is challenging due to its high reactivity, short lifetime (< 1 s), and low environmental concentration (Stone et al., 2012). After decades of efforts, tropospheric OH radicals can now be detected following the development of laser-induced fluorescence (LIF)–fluorescence assay with gas expansion (Hard et al., 1984), chemical ionization mass spectrometry (CIMS; Eisele et al., 1991), and open-path differential optical absorption spectrometry (Hausmann et al., 1997). The theory, advantages, and disadvantages of various measuring techniques have been discussed previously (Hard et al., 1979; Mao et al., 2012). Using these techniques, multiple campaigns have been conducted to measure the atmospheric OH concentrations in different regions around the globe. Figure 1 summarises the previous field observations of OH radicals in various environments.

OH observations are often compared with model simulations to evaluate whether a model has included the major OH sources and sinks. A summary of the results of the most recent studies is shown in Table 1 with the simulation to observation ratios ($R_{S/O}$). As concluded in previous reviews (Stone et al., 2012;

https://doi.org/10.5194/egusphere-2022-854
Preprint. Discussion started: 27 September 2022

Rohrer et al., 2014; Lu et al., 2019a), observed OH concentrations can generally be reproduced by box models under high NO conditions (NO > 1 ppb), such as at urban sites or within polluted air masses (Shirley et al., 2006; Griffith et al., 2016; Slater et al., 2020). However, discrepancies between model predictions and observations have often been found under low NO conditions (NO < 1 ppb). The model typically overpredicts OH concentrations in a low VOC environment and underpredicts them in a high biogenic VOC (BVOC) environment, as discussed below.

The model overestimation of OH has been found in various environments, including remote marine boundary layers and coastal, urban, and Arctic regions (Table 1). Previous studies have attributed the discrepancy to the overestimation of OH sources, missing OH sinks, and the uncertainties inherent in model simulation and observation. For example, model overestimation of OH has been found when dominant sources, such as HCHO and NO (Zhang et al., 2006), HONO (Kukui et al., 2014), and HO_2 (Kanaya et al., 2007a), are overestimated. In these cases, the overestimation of OH was resolved when these sources were better constrained in the model. Unmeasured VOCs have been proposed as the missing OH sinks, especially in aged air (McKeen et al., 1997; Carslaw et al., 1999; Berresheim, 2002; Creasey et al., 2003; Mauldin et al., 2010; Griffith et al., 2016). Previous studies have shown evidence of missing OH sinks in the forest (Hansen et al., 2014) and marine (Thames et al., 2020) regions, likely resulting from unmeasured organic compounds in biogenic ((Kaiser et al., 2016)) or oceanic (Thames et al., 2020) emissions and their oxidation products. In relation to potential overestimations caused by simulation and measurement uncertainties, some studies have shown that the overestimations fall within measurement uncertainties (McKeen et al., 1997, Carslaw et al., 1999), while others have suggested a possible sampling loss of OH (Mauldin et al., 2010) or a possible calibration bias due to low relative humidity (Mauldin et al., 2001).

Underestimations of OH by models have mostly been found in forest areas with high BVOC emissions (mostly isoprene) and low NO conditions. These underestimations have usually been attributed to missing OH sources (Tan et al., 2001; Lelieveld et al., 2008; Hofzumahaus et al., 2009; Whalley et al., 2011). To explain the missing sources, a series of new OH regeneration reactions under low NO conditions were proposed based on chamber experiments that investigated the oxidation of isoprene by

https://doi.org/10.5194/egusphere-2022-854
Preprint. Discussion started: 27 September 2022

OH. This mechanism, known as the Leuven isoprene mechanism (LIM1; Peeters et al., 2014), includes unimolecular reactions (Peeters et al., 2009; Da Silva, 2010; Fuchs et al., 2013; Novelli et al., 2020) and isomerisation of isoprene and/or its products (Peeters and Müller, 2010; Fuchs et al., 2014). With the adoption of this mechanism, the simulated OH concentration increased by 20%–30% in the forest region (Lew et al., 2020). Another breakthrough was the development of a new chemical scavenging technique in LIF instruments that was able to determine the interference to the instrument's background. Some studies have shown that the interference in LIF instruments can partly explain the previously observed high OH concentrations (Mao et al., 2012; Hens et al., 2014; Novelli et al., 2014a; Feiner et al., 2016; Woodward-Massey et al., 2020). With the adoption of interference scavenging and the LIM1 improved mechanism, measurements using LIF in an Alabama forest (Feiner et al., 2016) and CIMS in Amazon forests (Jeong et al., 2022) agreed with the OH concentration predicted by the model. However, the models in other studies continued to underestimate OH with the improved mechanism (Tan et al., 2019; Lew et al., 2020).

The industrialisation of the Pearl River Delta (PRD) region of south China over the past three decades has been accompanied by high anthropogenic emissions of air pollutants (Lu et al., 2013b), causing elevated concentrations of surface ozone (Wang et al., 2019b) and particulate matter (Yao et al., 2014). Measurements of OH in the PRD region that were taken using LIF at a forested site (Backgarden) indicated missing OH sources at this BVOC-rich site (Hofzumahaus et al., 2009; Lu et al., 2012). More recently, OH concentrations were measured at a suburban site in Shenzhen during autumn 2018 (Wang et al., 2019a; Wang et al., 2021) using a newly developed LIF instrument. The OH concentrations, which had an average value of 5.3×10^6 cm^{-3} around noon, were briefly presented with no comparison to modeled OH.

In the present study, we measured OH concentrations using quadrupole CIMS from October to November 2020 at a background site in Hong Kong. The study aimed to determine the OH concentrations in coastal south China and to investigate whether they could be simulated by a state-of-the-art chemical model under different airflow conditions. We first give a brief description of the site and OH measurement procedure, including the working theory of CIMS, calibration, uncertainties, and

https://doi.org/10.5194/egusphere-2022-854
Preprint. Discussion started: 27 September 2022

modelling setup. We then present the overall measurement results for different air masses and compare them with those found in previous studies. After this, we simulate OH concentrations using a box model constrained by comprehensive observations and discuss possible reasons for the model–observation discrepancy. Our measurements add to the limited database of ambient OH radical concentrations, while our analysis sheds light on possible missing OH sinks under low NO_x conditions.

2. Methodology

2.1 The Hok Tsui Supersite

Our field campaign was conducted at the Cape D'Aguilar (also known as Hok Tsui, HT) Air Quality Supersite, which is operated by the Hong Kong Environmental Protection Department, between 6 October and 24 November 2020. The HT Supersite (22°12'32" N, 114°15'12" E) is a coastal site located at the south-eastern tip of Hong Kong Island. The site is surrounded by ocean, vegetation, and scattered country roads (Figure 2) and is around 15 km away from the nearest urban centre. There is no strong anthropogenic emission source in the surrounding area apart from the ocean-going vessels travelling in nearby waters (Peng et al., 2022). Nonetheless, the site does occasionally receive polluted air masses from mainland China, including masses from the highly urbanised PRD region (Li et al., 2018; Peng et al., 2022).

We measured OH radicals, O_3, NO_x, CO, HONO, VOCs, oxygenated VOCs (OVOCs), relative humidity, temperature, NO_2 photolysis frequency (J_{NO2}), and aerosol size distribution. Table 2 summarises the measurement technique, resolution, and detection limits. The OH-CIMS was housed in an air-conditioned shelter in yard B together with the time-of-flight (ToF)-CIMS and ozone and NO_x analysers (Figure 2). J_{NO2} was measured on top of the shelter. The other species and the aerosol size distribution were measured inside the main station building in yard A, which was located around 10 m away from yard B (Figure 2). The backward trajectory was calculated at 1-hour intervals on sampling days at an elevation of 60 m above ground level using the MeteoInfoMap software package (meteothink.org, Wang, 2014; Wang, 2019).

https://doi.org/10.5194/egusphere-2022-854
Preprint. Discussion started: 27 September 2022

2.2 OH radical measurements

OH radical concentrations were indirectly measured using a custom-built quadrupole CIMS instrument. CIMS was originally developed by Eisele and Tanner (1991) and improved upon in subsequent works (Eisele and Tanner, 1993; Tanner and Eisele, 1995; Tanner et al., 1997). Detailed descriptions of CIMS measurement principles, configuration, optimisation, and calibration have been provided by Pu et al. (2020); here we only give a summary. The details of the technique, such as flow rates, reaction time, and concentrations, are shown in Table 3.

A schematic diagram of our OH-CIMS instrument is shown in Figure 3. The procedure was as follows. First, ambient air was drawn into the stainless steel inlet with a turbulence-reducing scoop by the inlet pump. The central part of the air in the stainless steel inlet was then drawn into the sample inlet, where OH was converted into H_2SO_4 by adding SO_2 to the sample flow. In the sheath flow, the NO_3^- reagent ion cluster was produced by passing an HNO_3-containing flow through a ^{210}Po ion source. The converted H_2SO_4 in the sample flow was then reacted with the excess NO_3^- cluster in the sheath flow and converted into an HSO_4^- ion cluster in the ionization chamber. The NO_3^- and HSO_4^- ion clusters further dissociated in the collisional dissociation chamber (CDC), refocused in the ion guide chamber (IGC), and were then detected by the detector in the ion detection chamber (IDC). In this case, HSO_4^- and NO_3^- were detected by the peak intensities at m/z = 97 (S_{97}) and m/z = 62 (S_{62}). The HSO_4^- ion concentration was determined based on relative signal strength (the S_{97}/S_{62} ratio) rather than absolute signal (S_{97}; Berresheim et al., 2000).

It should be noted that interference gases, such as ambient H_2SO_4, Criegee intermediates (Berresheim, 2002; Mauldin et al., 2012; Novelli et al., 2014b), and artificial OH produced by the ion source, also be converted into HSO_4^- and contribute to the signal S_{97}. To mitigate such interference, the scavenger gas (C_3F_6) and N_2 were added to the sample flow through electrically operated valves (see the pulsed flow in Figure 3) that automatically switched injection positions every 1 min. When a scavenger gas is added to the front injectors, ambient OH radicals are eliminated by the scavenger instead of reacting with SO_2 due to the higher concentration (~100 times) and faster reaction (Dubey et al., 1996) of C_3F_6 than of SO_2 in the sample flow. This allows the background signal (BS_{97}) contributed by the interference gases

https://doi.org/10.5194/egusphere-2022-854
Preprint. Discussion started: 27 September 2022

to be determined. When a scavenger gas is added to the rear injector, the ambient OH radicals and interference gases react with SO_2 to give the total signal (TS_{97}). Then, the ambient OH signal can be obtained by subtracting the signal contributed by interference (BS_{97}) from the total signal (TS_{97}). The measured OH concentration ([OH]) can be calculated using the following equation (E1):

$$[OH] = \frac{1}{C} \times \frac{TS_{97} - BS_{97}}{S_{64}} \text{ (E1)}$$

where *c* is the calibration factor obtained from calibration that was performed using the calibrator shown in Figure 3. The calibration is based on the production of OH radicals through the photolysis of water vapor by 184.9 nm light in the airflow through the calibrator (E2).

$$H_2O + hv(184.9\ nm) \rightarrow H + OH \text{ (E2)}$$

$$H + O_2 + M \rightarrow M + HO_2 \text{ (E3)}$$

$$[OH] = [H_2O] * \sigma_{H_2O} * \Phi * It \text{ (E4)}$$

The OH concentration produced by the calibrator is calculated by E4. σ_{H_2O} (= 7.22×10^{-20} cm^2; Cantrell et al., 1997) is the photolysis cross-section of water vapor, while Φ represents the photolysis quantum yield, which is assumed to be 1 (Kürten et al., 2012). The H_2O concentration was calculated using the measured temperature and dew point temperatures of the calibrating air using the ideal gas law. The photon flux (It) was determined using the chemical actinometry method (Kürten et al., 2012). In this study, the It values were measured before and after the field campaign and no significant difference was found. Calibration was carried out at least every two days during the campaign, as well as before and after any changes in settings. The difference in calibration factors was included by the calibration accuracy.

The overall calibration accuracy was estimated at 38%, by calculation that took into account the uncertainty of all of the parameters measured in E4 during the calibration process and the variation in calibration factors during the campaign. The detection limit is approximately 1.5×10^5 cm^{-3} (signal-to-noise ratio of 2) in the laboratory. However, due to variation in the concentrations of H_2SO_4 and other interference gases in the ambient air, the detection limit for *in situ* measurement may change along with the ambient conditions and higher than the detection limit in the laboratory. The daytime and nighttime average detection limits in this campaign were 1.0 and 0.7×10^6 cm^{-3}, respectively.

https://doi.org/10.5194/egusphere-2022-854
Preprint. Discussion started: 27 September 2022

2.3 Box modelling

The Framework for 0-D Atmospheric Modelling (F0AM) using the Master Chemical Mechanism (MCM) v3.3.1 (Wolfe et al., 2016) was used to simulate OH concentrations. MCM v3.3.1 (http://mcm.leeds.ac.uk/MCM) is a near-explicit chemical mechanism that includes over 17,000 elementary reactions of 6700 primary, secondary, and radical species (Jenkin et al., 2015). The isoprene degradation mechanisms, and in particular the HO_x recycling mechanisms, are included in MCM v3.3.1. The MCM mechanism has been used in previous studies to investigate OH chemistry in different environments, including forests (Stone et al., 2011), urban areas (Slater et al., 2020), suburban areas (Tan et al., 2018), and coastal regions (Sommariva et al., 2004). Observational data (shown in Table S1) were used to constrain the model. These data included VOCs, OVOCs, SO_2, NO_x, CO, O_3, HONO, and meteorological parameters (temperature, relative humidity, pressure, and J_{NO2}). The photolysis frequencies for other species were calculated as a function of the solar zenith angle (φ) using E5 and then scaled using observed versus modelled J_{NO2}.

$$J = l \times (cos\varphi)^m \times e^{-n \times sec\,\varphi} \quad \text{(E5)}$$

The values of the *l*, *m*, and *n* parameters for photolysis frequency with respect to different species were drawn from Saunders et al. (2003).

In this study, the first-order physical loss process, with a 24-hour lifetime for all species, was included in the model to represent physical processes such as advection, deposition, and dilution (Wolfe et al., 2016; (Chen et al., 2022)). The physical loss process has a negligible influence on OH simulation because the OH concentrations are controlled by fast *in situ* chemistry.

The heterogeneous uptake of HO_2 by aerosols was included in the model by assuming a pseudo-first-order loss of HO_2 (E6–E8; (Jacob, 2000):

$$\frac{d[HO_2]}{dt} = -k_{HO_2}[HO_2] \quad \text{(E6)}$$

$$k_{HO_2} = \frac{V_{HO_2} \times S_a \times \gamma_{HO_2}}{4} \quad \text{(E7)}$$

$$V_{HO_2} = \sqrt{\frac{8RT}{\pi \times MW_{HO_2}}} \quad \text{(E8)}$$

https://doi.org/10.5194/egusphere-2022-854
Preprint. Discussion started: 27 September 2022

where k_{HO_2} is the first-order loss rate coefficient of HO_2 by aerosol uptake, γ_{HO2} is the effective HO_2 uptake coefficient (= 0.1 for the base model run; (Guo et al., 2019), V_{HO_2} is the mean molecular velocity of HO_2, S_a is the aerosol surface area concentration measured by scanning mobility particle sizing (SMPS), and MW_{HO_2} (= 17 g/mol) is the molecular weight of HO_2. We assumed in the model that the products of heterogeneous HO_2 loss would not participate in further reactions (Guo et al., 2019).

The observation data were averaged every 10 mins for the model input. Any missing values were calculated assuming linear interpolation. The measured concentrations of NO and NO_2 were used to constrain the model, with the NO/NO_2 ratio calculated based on the family conversion, as recommended in a previous study (Wolfe et al., 2016; Figure S1). Due to the clean condition of the coastal air, some of the reactive alkenes and long-chain alkanes were below detection limits. For the simulation of those compounds, we used concentrations that were half of the detection limits. The measured VOCs were further divided into those of anthropogenic origin (AVOCs) and biogenic origin (BVOCs). The AVOCs included alkanes (C_2–C_8), benzene, and TEXs (toluene, ethylbenzene, and xylenes), which covered the dominant species originating from petroleum gas and industrial solvent evaporation (Tang et al., 2008), while the BVOCs included isoprene, terpene, pinene, and limonene. The majority (> 95%) of the measured OVOCs in this study were C_1–C_3 aldehydes, ketones, and acids. For each run, a three-day spin-up was performed to create a stable model environment and to avoid the uncertainty of unconstrained species (Carslaw et al., 1999).

3. Results and Discussion

3.1 Overview of observations

Figure 4 shows the time series of observed OH concentrations, along with the concentrations of other trace gases and the meteorological parameters, during the campaign. The weather conditions during the study featured relatively high temperatures, high relative humidity (RH), and strong solar radiation, consistent with previously reported autumn observations at the same site (Li et al., 2018; Peng et al., 2022). The air temperature ranged from 20°C to 30°C and RH ranged from 40% to 96%. The photolysis frequency of NO_2 (J_{NO2}) peaked at 8×10^{-3} s^{-1} around noon on sunny days but decreased to 2×10^{-3} s^{-1} on cloudy days. The observed OH concentrations were mostly above the detection limit during the

https://doi.org/10.5194/egusphere-2022-854
Preprint. Discussion started: 27 September 2022

daytime but fell closer to the detection limit at night. The OH concentrations showed a distinct diurnal pattern and a positive correlation with J_{NO2} (R^2 = 0.67, Figure S2). The daily maximum OH concentration varied from 2.1 × 10^6 cm^{-3} on 21 November, accompanying the lowest level of solar radiation, to 15.4 × 10^6 cm^{-3} on 7 November which was measured during a pollution episode. The pollution episode began on the evening of 6 November and featured a maximum concentration of 174.0 ppb O_3, 8.7 ppb NO, 22.7 ppb NO_2, 36.5 ppb total VOCs, and 48.1 ppb total OVOCs. The OH concentration peaked the next day (7 Nov). This suggests abundant OH sources and fast radical propagation under high-NO_x and high-VOC conditions.

Figure 5 shows the average diurnal profiles of OH and other representative species. On average, the maximum OH concentration was 4.9 ± 2.1 × 10^6 (1σ) cm^{-3}. As shown in Table 1, the OH concentrations at our site were comparable to those reported in previous field studies conducted at tropical coastal sites. For example, the reported OH maximum concentration was 4.5 × 10^6 cm^{-3} in the low-altitude remote tropical troposphere (Brune et al., 2020). In a study conducted in autumn at a suburban site in Shenzhen, approximately 50 km away from our site, an OH diurnal maximum concentration of 5.3 × 10^6 cm^{-3} was observed (Wang et al., 2021). Figure 5 also shows the average diurnal patterns of the other trace gases measured. The primary precursor of OH, HONO, peaked in the morning at 0.21 ± 0.09 ppb around 7:00 local time (LT), while O_3 peaked in the afternoon (70 ± 20 ppb at around 16:00 LT). The average NO and NO_2 concentrations reached a maximum of 1.2 ± 1.6 ppb at around 10:00 LT and 4.9 ± 3.2 ppb at around 18:00 LT, respectively. Isoprene showed a diurnal pattern similar to that of J_{NO2} and OH, peaking at 0.5 ± 0.4 ppb at noon. The average concentrations of all of the measured species during the campaign are shown in Table S1.

Figure 6 shows the hourly backward trajectories over the whole campaign. Consistent with previous studies conducted at HT in the same season (Li et al., 2018; Peng et al., 2022), the air masses were dominated by continental air masses containing high concentrations of pollutants (Figure 6a) and less polluted coastal air masses (Figure 6c). In this campaign, we did not encounter oceanic air masses from the south. The average noontime OH concentration was 5.0 ± 2.2 × 10^6 cm^{-3} in the continental air mass cluster (Figure 6b) and 3.3 ± 1.6 × 10^6 cm^{-3} in the coastal air (Figure 6d).

https://doi.org/10.5194/egusphere-2022-854
Preprint. Discussion started: 27 September 2022

3.2 Model–observation comparison

To investigate the performance of the MCM box model in simulating OH chemistry at our site, we selected 4 days featuring the continental air mass (8, 21, 22, and 23 Oct) and 4 days featuring the coastal air mass (25–27 Oct, 5 November). We also selected 10 October as a specific case due to the shifting continental and coastal air masses within the same day during the daytime. These days were selected for model analysis because they comprised relatively complete chemical data that could be used to constrain the model.

3.2.1 Selected continental air mass cases

Figure 7 shows the comparison between the simulated and observed OH concentrations for the selected cases in the continental and coastal air masses (4 days each). The simulated OH concentrations of the four continental cases (8 October and 21–23 October) were mostly within the OH measurement uncertainty (2σ), with a daytime average $R_{S/O}$ of 0.97 (Figure 8) and a range from 0.87 to 1.02 (Figure 7). High NO_x (~ 5 ppb) and VOCs (~17 ppb) concentrations were measured on these days (Figure 8, Table S1). Therefore, in the continental polluted air mass, the existing MCM mechanism reproduced the observed OH concentrations well. On these days, the reaction between HO_2 and NO was the dominant OH formation pathway (78%), followed by HONO photolysis (10%), O_3 photolysis (5%), the reaction between ozone and HO_2 (2%), and alkene ozonolysis (1%; Table 4 and Figure S3). This is similar to the findings of previous studies in the PRD conducted during autumn under polluted conditions (Tan et al., 2019). The removal of OH occurs mainly through its reaction with non-methane hydrocarbons (NMHCs; ~63%), CO (20%), NO_2 (10%), and CH_4 (4%; Table 4). Note that the reactions with NMHCs, CO, and CH_4 produce peroxy (HO_2 and RO_2) radicals (Stone et al., 2012). The simulated OH reactivity was 8.7 ± 0.7 s^{-1} on average for continental air masses (Figure S4a), which is comparable to the OH reactivity measured at suburban sites (which ranged from 5 to 30 s^{-1}) but lower than that measured at the urban sites (which ranged from 10 to 100 s^{-1}; Yang et al., 2016 and references therein).

3.2.2 Selected coastal air mass cases

The diurnal OH patterns in the coastal air mass category (25–27 October and 5 November) were not

https://doi.org/10.5194/egusphere-2022-854
Preprint. Discussion started: 27 September 2022

well reproduced by the model (Figure 7), in contrast to the continental air mass cases. The simulated results overestimated the observed OH concentration, with the daytime average $R_{S/O}$ of 1.73 (Figure 8) for these 4 case days (range 1.48 to 2.53; Figure 7). The coastal air masses showed significantly ($p < 0.05$) lower NO_x (−63%), AVOCs (−47%), BVOCs (−50%), OVOCs (−23%), and CO (−31%) concentrations compared with the continental cases (Figure 8, Table S1). The HO_2 and NO reaction was still the dominant source (64%) of OH in the coastal air masses, like in the continental air mass cases, but in a lower proportion than on continental days due to the lower NO concentration (Table 4 and Figure S3). The other major OH sources were HONO photolysis (15%), O_3 photolysis (10%), and the reaction between ozone and HO_2 (4%). The simulated OH reactivity was 5.4 ± 0.33 s^{-1} on average for the coastal case (Figure S4b), which was lower than that of the continental polluted air mass (8.7 ± 0.7 s^{-1}). As discussed below in Section 3.3, low OH reactivity could have been the cause of the model's overestimation of OH concentrations on the coastal case days. The model's overestimation of OH in coastal air masses indicates gaps in our knowledge about OH sources or sinks in relatively clean conditions with low NO_x and VOCs.

3.2.3 The 10 October case day

During the day on 10 October, our site received continental air masses between sunrise and noon and coastal air masses between noon and sunset. This served as another case that could be used to check the model's performance on continental versus coastal air masses within the same day. On 10 October, the $R_{S/O}$ changed from 1.08 in the morning to 1.70 in the afternoon, driven by the air mass drift during continuous measurement without interruption (Figure 9). As with the continental and coastal air mass results shown above, the afternoon of 10 October showed significantly ($p < 0.05$) lower concentrations of NO (−50%), NO_2 (−68%), AVOCs (−42%), BVOCs (−27%), and OVOCs (−12%) compared with the morning (Table 4). With lower NO, the fraction of OH produced from HO_2 and NO reaction was also lower in the afternoon (54%) than in the morning (71%; Table 4 and Figure S3). Similarly, the simulated OH reactivity was lower in the afternoon (8.1 ± 2.0 s^{-1} on average) than in the morning (11.3 ± 1.1 s^{-1} on average; Figure S4c).

3.3 Discussion on the model–observation discrepancy

https://doi.org/10.5194/egusphere-2022-854
Preprint. Discussion started: 27 September 2022

As discussed in the introduction, the model's overestimation of OH could have been caused by multiple factors, including uncertainties in OH measurements (McKeen et al., 1997; Carslaw et al., 1999; Mauldin et al., 2001; Mauldin et al., 2010), overestimation of OH sources (HO_2 and HONO; Kanaya, et al., 2007; Zhang et al., 2006), and underestimation of OH sinks (Berresheim, 2002; Creasey et al., 2003; Mauldin et al., 2010; Griffith et al., 2016). The possible reasons for the model's overestimation of OH in coastal air are discussed below.

The OH measurement uncertainties in our study were described in Section 2.2. The model's overestimation of OH in coastal air masses exceeded the measurement uncertainties (Figure 7). The main sources of OH in the coastal air masses were the HO_2 + NO reaction (64%), HONO photolysis (15%), O_3 photolysis (10%), and the reaction between ozone and HO_2 (4%). In the model, NO, HONO, and O_3 were constrained by observations. To check whether the overestimation could be explained by a larger uptake of HO_2 onto aerosol, we conducted a sensitivity run by increasing the aerosol uptake of HO_2 (RUNγ1, Figure S5). In RUNγ1, the HO_2 uptake coefficient was set to unity. The simulated HO_2 concentration in RUNγ1 decreased by 34% compared with the base case (RUNBase). Correspondingly, the simulated OH $R_{S/O}$ decreased to 1.42 in RUNγ1, as compared with 1.70 in RUNBase. This indicates that the heterogeneous uptake of HO_2 is not sufficient to explain the OH discrepancy. A likely explanation is the low conversion efficiency from HO_2 to OH at low NO concentrations, as was found in a previous study (Sommariva et al., 2004).

We propose that the model's overestimation of OH could have been caused by unmeasured species that were not included in the model as OH sinks. To account for these OH sinks and to investigate which factors were important in relation to these sinks, we added a "fake" reaction into the model with the reactivity of k_{miss} (s^{-1}) and assumed that the reaction product would not participate in further reactions. Assuming a pseudo-steady state of OH during the daytime (P = k[OH]), k_{miss} was calculated as follows:

$$k_{miss} = \frac{P_{constrain}}{[OH_{obs}]} - \frac{P_{constrain}}{[OH_{sim}]} \quad \text{(E9)}$$

where $P_{constrain}$ is the model's calculated OH production rates, with OH constrained by observations; $[OH_{obs}]$ is the observed OH concentration; and $[OH_{sim}]$ is the OH concentration simulated in RUNBase. After introducing the OH removal reaction with k_{miss} into the model (RUNKmiss, Figure S6),

https://doi.org/10.5194/egusphere-2022-854
Preprint. Discussion started: 27 September 2022

the model better reproduced the observed OH concentrations on the coastal case days, with daytime $R_{S/O}$ close to unity (Figure S6). This supported our estimate of k_{miss}. The average daytime k_{miss} for the coastal cases was 4.2 ± 2.2 s^{-1}, which corresponds to 43% of the total calculated reactivity.

We also further explored the dependence of k_{miss} on different trace gases. Figure 10a shows the correlation between k_{miss} and NO concentration for the nine case days (including 10 October) between 09:00 and 15:00. At NO > 0.5 ppb, k_{miss} is close to zero. At NO < 0.5 ppb, k_{miss} tended to increase with decreasing NO. Similarly, k_{miss} approached zero at high concentrations of NO_2 (> 2.5 ppb), TEXs (> 0.25 ppb), and AVOCs (> 5 ppb; Figure 10) and increased with decreasing concentrations of NO_2, TEXs, and AVOCs. High k_{miss} also typically occurred at low toluene/benzene ratios and low C_2H_2/CO ratios, which are indicators of an aged air mass (Figure 10; Xiao et al., 2007; Kuyper et al., 2020) Therefore, our results suggested that the aged coastal air masses could have contained unmeasured species such as oxygenated organic molecules (OOMs; Nie et al., 2022) and ocean-emitted gases (Thames et al., 2020) that contributed to the missing OH reactivity, causing the model to overestimate OH concentrations on the coastal case days.

Summary and conclusion

In this study, we measured OH concentrations using CIMS at a coastal site in Hong Kong in autumn 2020 to gain insights into the atmospheric oxidative capacity and to evaluate the performance of a box model in the coastal atmosphere. The daily maximum OH concentration ranged from 2.1 to 15.4 × 10^6 cm^{-3} over the whole campaign, with an average of 4.9 ± 2.1 × 10^6 cm^{-3}. The air masses were categorised into two groups based on their backward air trajectories: (1) continental masses, which contained high concentrations of NO_x and VOCs, and (2) coastal masses, which contained low concentrations of NO_x and VOCs. The observed OH concentration in the continental air parcels was on average 52% higher than in the coastal air parcels. The F0AM box model with comprehensive observational constraints generally reproduced the observed OH in the continental cases during the daytime, with a simulated/observed OH ratio ($R_{S/O}$) of 0.97 on average. However, the model significantly overestimated OH concentrations in the coastal cases, with an $R_{S/O}$ of 1.70 on average during the daytime. We attributed this overestimation to a missing OH reactivity in the aged coastal air parcels that was not

https://doi.org/10.5194/egusphere-2022-854
Preprint. Discussion started: 27 September 2022

accounted for in the model. The missing OH reactivity was estimated at 4.2 ± 2.2 s^{-1} on average between 09:00 and 15:00 and was especially larger under low NO_x, low AVOCs, and aged air conditions. This result suggests that unknown products from AVOC oxidation or unknown OH-reacting gases emitted from oceans could contribute to the missing OH reactivity in aged coastal air masses. The missing OH reactivity in the model could cause an overestimation of the formation of secondary aerosols, such as sulfate and nitrate, while the impacts would be even more complicated if the missing chemical species participated in ozone formation. Further studies are necessary to pin down the exact cause(s) of the OH overestimation, for example, through measurements of other VOC oxidation products and ocean-emitted trace gases.

Data availability. All of the data used to produce this paper can be obtained by contacting Tao Wang (two.wang@polyu.edu.hk).

Supplement. The online supplement for this article is available at:

Author contributions. TW initially conceived of the project. TW and ZW planned and organised the overall field campaign at Hok Tsui. ZZ conducted the OH measurements using CIMS, with contributions from TW and ZW. YC performed the aerosol size distribution measurements. YQ performed the OVOC measurements using PTR-MS. MX and YC performed the HONO measurements using ToF-CIMS. YW assisted with HONO calibration. ZZ performed the box model analysis and sensitivity test with contributions from EX and QC. ZZ, TW, and QC analysed the data and interpreted the results, with contributions from MX. ZZ, TW and QC wrote the paper. All of the authors reviewed and commented on the paper.

Competing interests. One author (Tao Wang) is a member of the editorial board of Atmospheric Chemistry and Physics. The peer-review process was guided by an independent editor, and the authors have no other competing interests to declare.

Acknowledgments

We thank David Tanner, Dr Wei Pu, and Dr Weihao Wang for developing the OH CIMS. We are also grateful to the Environmental Protection Department of Hong Kong, for loaning the CIMS instrument and providing access to its station and data on trace gases, and to the Hong Kong Observatory, for supplying meteorology data.

https://doi.org/10.5194/egusphere-2022-854
Preprint. Discussion started: 27 September 2022

Financial support. This research was financially supported by the Hong Kong Research Grants Council (T24-504/17-N and 15223221).

https://doi.org/10.5194/egusphere-2022-854
Preprint. Discussion started: 27 September 2022

Reference:

Berresheim, H.: Gas-aerosol relationships of H_2SO_4 , MSA, and OH: Observations in the coastal marine boundary layer at Mace Head, Ireland, J. Geophys. Res., 107, 8100, https://doi.org/10.1029/2000JD000229, 2002.

Berresheim, H., Elste, T., Plass-Dülmer, C., Eiseleb, F. ., and Tannerb, D. .: Chemical ionization mass spectrometer for long-term measurements of atmospheric OH and H_2SO_4, Int. J. Mass Spectrom., 202, 91–109, https://doi.org/10.1016/S1387-3806(00)00233-5, 2000.

Berresheim, H., McGrath, J., Adam, M., Mauldin, R. L., Bohn, B., and Rohrer, F.: Seasonal measurements of OH, NO_x, and $J_{(O1D)}$ at Mace Head, Ireland, Geophys. Res. Lett., 40, 1659–1663, https://doi.org/10.1002/grl.50345, 2013.

Berresheim, H., Adam, M., Monahan, C., O'dowd, C., Plane, J. M. C. C., Bohn, B., Rohrer, F., O'Dowd, C., Plane, J. M. C. C., Bohn, B., and Rohrer, F.: Missing SO_2 oxidant in the coastal atmosphere? - Observations from high-resolution measurements of OH and atmospheric sulfur compounds, Atmos. Chem. Phys., 14, 12209–12223, https://doi.org/10.5194/acp-14-12209-2014, 2014.

Bloss, W. J., Lee, J. D., Heard, D. E., Salmon, R. A., Bauguitte, S. J.-B., Roscoe, H. K., and Jones, A. E.: Observations of OH and HO_2 radicals in coastal Antarctica, Atmos. Chem. Phys., 7, 4171–4185, https://doi.org/10.5194/acp-7-4171-2007, 2007.

Brune, W. H., Miller, D. O., Thames, A. B., Allen, H. M., Apel, E. C., Blake, D. R., Bui, T. P., Commane, R., Crounse, J. D., Daube, B. C., Diskin, G. S., DiGangi, J. P., Elkins, J. W., Hall, S. R., Hanisco, T. F., Hannun, R. A., Hintsa, E. J., Hornbrook, R. S., Kim, M. J., McKain, K., Moore, F. L., Neuman, J. A., Nicely, J. M., Peischl, J., Ryerson, T. B., St. Clair, J. M., Sweeney, C., Teng, A. P., Thompson, C., Ullmann, K., Veres, P. R., Wennberg, P. O., and Wolfe, G. M.: Exploring Oxidation in the Remote Free Troposphere: Insights From Atmospheric Tomography (ATom), J. Geophys. Res. Atmos., 125, 1–17, https://doi.org/10.1029/2019JD031685, 2020.

Cantrell, C. A., Zimmer, A., Tyndall, G. S., Cantrell, A., and Tyndall, S.: Absorption cross sections for water vapor from 183 to 193 nm, Geophys. Res. Lett., 24, 2195–2198, https://doi.org/10.1029/97GL02100, 1997.

Carslaw, N., Creasey, D. J. J., Heard, D. E. E., Lewis, A. C. C., McQuaid, J. B. B., Pilling, M. J. J.,

https://doi.org/10.5194/egusphere-2022-854
Preprint. Discussion started: 27 September 2022

Monks, P. S. S., Bandy, B. J. J., and Penkett, S. A. A.: Modeling OH, HO_2 , and RO_2 radicals in the marine boundary layer: 1. Model construction and comparison with field measurements, J. Geophys. Res. Atmos., 104, 30241–30255, https://doi.org/10.1029/1999JD900783, 1999.

Chen, Q., Xia, M., Peng, X., Yu, C., Sun, P., Li, Y., Liu, Y., Xu, Z., Xu, Z., Wu, R., Nie, W., Ding, A., Zhao, Y., and Wang, T.: Large Daytime Molecular Chlorine Missing Source at a Suburban Site in East China, J. Geophys. Res. Atmos., 127, 1–19, https://doi.org/10.1029/2021JD035796, 2022.

Chen, S., Ren, X., Mao, J., Chen, Z., Brune, W. H., Lefer, B., Rappenglück, B., Flynn, J., Olson, J., and Crawford, J. H.: A comparison of chemical mechanisms based on TRAMP-2006 field data, Atmos. Environ., 44, 4116–4125, https://doi.org/10.1016/j.atmosenv.2009.05.027, 2010.

Creasey, D. J., Evans, G. E., Heard, D. E., and Lee, J. D.: Measurements of OH and HO_2 concentrations in the Southern Ocean marine boundary layer, J. Geophys. Res. Atmos., 108, 1–12, https://doi.org/10.1029/2002jd003206, 2003.

Dubey, M. K., Hanisco, T. F., Wennberg, P. O., and Anderson, J. G.: Monitoring potential photochemical interference in laser-induced fluorescence measurements of atmospheric OH, Geophys. Res. Lett., 23, 3215–3218, https://doi.org/10.1029/96GL03008, 1996.

Dusanter, S., Vimal, D., Stevens, P. S., Volkamer, R., and Molina, L. T.: Measurements of OH and HO_2 concentrations during the MCMA-2006 field campaign – Part 1: Deployment of the Indiana University laser-induced fluorescence instrument, Atmos. Chem. Phys., 9, 1665–1685, https://doi.org/10.5194/acp-9-1665-2009, 2009a.

Dusanter, S., Vimal, D., Stevens, P. S., Volkamer, R., Molina, L. T., Baker, A., Meinardi, S., Blake, D., Sheehy, P., Merten, A., Zhang, R., Zheng, J., Fortner, E. C., Junkermann, W., Dubey, M., Rann, T., Eichinger, B., Lewandowski, P., Prueger, J., and Holder, H.: Measurements of OH and HO_2 concentrations during the MCMA-2006 field campaign - Part 2: Model comparison and radical budget, Atmos. Chem. Phys., 9, 6655–6675, https://doi.org/10.5194/acp-9-6655-2009, 2009b.

Eisele, F. L. and Tanner, D. J.: Measurement of the gas phase concentration of H_2SO_4 and methane sulfonic acid and estimates of H_2SO_4 production and loss in the atmosphere, J. Geophys. Res. Atmos., 98, 9001–9010, https://doi.org/10.1029/93JD00031, 1993.

Eisele, F. L., Tanner, D. J., and Autoridad Nacional del Servicio Civil: Ion-assisted tropospheric OH measurements, J. Geophys. Res., 96, 9295, https://doi.org/10.1029/91JD00198, 1991.

https://doi.org/10.5194/egusphere-2022-854
Preprint. Discussion started: 27 September 2022

Emmerson, K. M., Carslaw, N., Carslaw, D. C., Lee, J. D., McFiggans, G., Bloss, W. J., Gravestock, T., Heard, D. E., Hopkins, J., Ingham, T., Pilling, M. J., Smith, S. C., Jacob, M., and Monks, P. S.: Free radical modelling studies during the UK TORCH Campaign in Summer 2003, Atmos. Chem. Phys., 7, 167–181, https://doi.org/10.5194/acp-7-167-2007, 2007.

Feiner, P. A., Brune, W. H., Miller, D. O., Zhang, L., Cohen, R. C., Romer, P. S., Goldstein, A. H., Keutsch, F. N., Skog, K. M., Wennberg, P. O., Nguyen, T. B., Teng, A. P., DeGouw, J., Koss, A., Wild, R. J., Brown, S. S., Guenther, A., Edgerton, E., Baumann, K., and Fry, J. L.: Testing atmospheric oxidation in an Alabama forest, J. Atmos. Sci., 73, 4699–4710, https://doi.org/10.1175/JAS-D-16-0044.1, 2016.

Fuchs, H., Hofzumahaus, A., Rohrer, F., Bohn, B., Brauers, T., Dorn, H. P., Häseler, R., Holland, F., Kaminski, M., Li, X., Lu, K., Nehr, S., Tillmann, R., Wegener, R., and Wahner, A.: Experimental evidence for efficient hydroxyl radical regeneration in isoprene oxidation, Nat. Geosci., 6, 1023–1026, https://doi.org/10.1038/ngeo1964, 2013.

Fuchs, H., Acir, I. H., Bohn, B., Brauers, T., Dorn, H. P., Häseler, R., Hofzumahaus, A., Holland, F., Kaminski, M., Li, X., Lu, K., Lutz, A., Nehr, S., Rohrer, F., Tillmann, R., Wegener, R., and Wahner, A.: OH regeneration from methacrolein oxidation investigated in the atmosphere simulation chamber SAPHIR, Atmos. Chem. Phys., 14, 7895–7908, https://doi.org/10.5194/acp-14-7895-2014, 2014.

Fuchs, H., Albrecht, S., Acir, I. H., Bohn, B., Breitenlechner, M., Dorn, H. P., Gkatzelis, G. I., Hofzumahaus, A., Holland, F., Kaminski, M., Keutsch, F. N., Novelli, A., Reimer, D., Rohrer, F., Tillmann, R., Vereecken, L., Wegener, R., Zaytsev, A., Kiendler-Scharr, A., and Wahner, A.: Investigation of the oxidation of methyl vinyl ketone (MVK) by OH radicals in the atmospheric simulation chamber SAPHIR, Atmos. Chem. Phys., 18, 8001–8016, https://doi.org/10.5194/acp-18-8001-2018, 2018.

Giorio, C., Doussin, J., D'Anna, B., Mas, S., Filippi, D., Denjean, C., Mallet, M. D., Bourrianne, T., Burnet, F., Cazaunau, M., Chikwililwa, C., Desboeufs, K., Feron, A., Michoud, V., Namwoonde, A., Andreae, M. O., Piketh, S. J., and Formenti, P.: Butene Emissions From Coastal Ecosystems May Contribute to New Particle Formation, Geophys. Res. Lett., 49, https://doi.org/10.1029/2022gl098770, 2022.

Griffith, S. M., Hansen, R. F., Dusanter, S., Stevens, P. S., Alaghmand, M., Bertman, S. B., Carroll,

https://doi.org/10.5194/egusphere-2022-854
Preprint. Discussion started: 27 September 2022

M. A., Erickson, M., Galloway, M., Grossberg, N., Hottle, J., Hou, J., Jobson, B. T., Kammrath, A., Keutsch, F. N., Lefer, B. L., Mielke, L. H., O'Brien, A., Shepson, P. B., Thurlow, M., Wallace, W., Zhang, N., and Zhou, X. L.: OH and HO_2 radical chemistry during PROPHET 2008 and CABINEX 2009 - Part 1: Measurements and model comparison, Atmos. Chem. Phys., 13, 5403–5423, https://doi.org/10.5194/acp-13-5403-2013, 2013.

Griffith, S. M., Hansen, R. F., Dusanter, S., Michoud, V., Gilman, J. B., Kuster, W. C., Veres, P. R., Graus, M., de Gouw, J. A., Roberts, J., Young, C., Washenfelder, R., Brown, S. S., Thalman, R., Waxman, E., Volkamer, R., Tsai, C., Stutz, J., Flynn, J. H., Grossberg, N., Lefer, B., Alvarez, S. L., Rappenglueck, B., Mielke, L. H., Osthoff, H. D., and Stevens, P. S.: Measurements of hydroxyl and hydroperoxy radicals during CalNex-LA: Model comparisons and radical budgets, J. Geophys. Res., 121, 4211–4232, https://doi.org/10.1002/2015JD024358, 2016.

Guo, J., Wang, Z., Tao Wang, and Zhang, X.: Theoretical evaluation of different factors affecting the HO_2 uptake coefficient driven by aqueous-phase first-order loss reaction, Sci. Total Environ., 683, 146–153, https://doi.org/10.1016/j.scitotenv.2019.05.237, 2019.

Handisides, G. M., Plass-Dülmer, C., Gilge, S., Bingemer, H., and Berresheim, H.: Hohenpeissenberg Photochemical Experiment (HOPE 2000): Measurements and photostationary state calculations of OH and peroxy radicals, Atmos. Chem. Phys., 3, 1565–1588, https://doi.org/10.5194/acp-3-1565-2003, 2003.

Hansen, R. F., Griffith, S. M., Dusanter, S., Rickly, P. S., Stevens, P. S., Bertman, S. B., and Carroll, M. A.: Measurements of total hydroxyl radical reactivity during CABINEX 2009 – Part 1 : field measurements, Atmos. Chem. Phys., 2923–2937, https://doi.org/10.5194/acp-14-2923-2014, 2014.

Hard, T. M., O'Brien, R. J., Cook, T. B., and Tsongas, G. A.: Interference suppression in HO fluorescence detection, Appl. Opt., 18, 3216, https://doi.org/10.1364/AO.18.003216, 1979.

Hard, T. M., O'Brien, R. J., Chan, C. Y., and Mehrabzadeh, A. A.: Tropospheric Free Radical Determination by FAGE, Environ. Sci. Technol., 18, 768–777, https://doi.org/10.1021/es00128a009, 1984.

Hausmann, M., Brandenburger, U., and Brauers, T.: Detection of tropospheric OH radicals by long-path differential-optical-absorption spectroscopy: Experimental setup, accuracy, and precision, J. Geophys. Res., 102, 11–16, 1997.

https://doi.org/10.5194/egusphere-2022-854
Preprint. Discussion started: 27 September 2022

Hens, K., Novelli, A., Martinez, M., Auld, J., Axinte, R., Bohn, B., Fischer, H., Keronen, P., Kubistin, D., Nölscher, A. C., Oswald, R., Paasonen, P., Petäjä, T., Regelin, E., Sander, R., Sinha, V., Sipilä, M., Taraborrelli, D., Tatum Ernest, C., Williams, J., Lelieveld, J., and Harder, H.: Observation and modelling of HOx radicals in a boreal forest, Atmos. Chem. Phys., 14, 8723–8747, https://doi.org/10.5194/acp-14-8723-2014, 2014.

Hofzumahaus, A., Rohrer, F., Lu, K., Bohn, B., Brauers, T., Chang, C.-C. C. C., Fuchs, H., Holland, F., Kita, K., Kondo, Y., Li, X., Lou, S., Shao, M., Zeng, L., Wahner, A., and Zhang, Y.: Amplified trace gas removal in the troposphere, Science (80-.)., 324, 1702–1704, https://doi.org/10.1126/science.1164566, 2009.

Holland, F., Hofzumahaus, A., Schäfer, J., Kraus, A., and Pätz, H. W.: Measurements of OH and HO2 radical concentrations and photolysis frequencies during BERLIOZ, J. Geophys. Res. Atmos., 108, https://doi.org/10.1029/2001jd001393, 2003.

Ivanov, A. V., Gershenzon, Y. M., Gratpanche, F., Devolder, P., and Sawerysyn, J.-P.: Heterogeneous loss of OH on NaCl and NH_4NO_3 at tropospheric temperatures, Ann. Geophys., 14, 659–664, https://doi.org/10.1007/s00585-996-0659-5, 1996.

Jacob, D. J.: Heterogeneous chemistry and tropospheric ozone, Atmos. Environ., 34, 2131–2159, https://doi.org/10.1016/S1352-2310(99)00462-8, 2000.

Jenkin, M. E., Young, J. C., and Rickard, A. R.: The MCM v3.3.1 degradation scheme for isoprene, Atmos. Chem. Phys., 15, 11433–11459, https://doi.org/10.5194/acp-15-11433-2015, 2015.

Jeong, D., Seco, R., Emmons, L., Schwantes, R., Liu, Y., McKinney, K. A., Martin, S. T., Keutsch, F. N., Gu, D., Guenther, A. B., Vega, O., Tota, J., Souza, R. A. F. F., Springston, S. R., Watson, T. B., and Kim, S.: Reconciling Observed and Predicted Tropical Rainforest OH Concentrations, J. Geophys. Res. Atmos., 127, 1–18, https://doi.org/10.1029/2020JD032901, 2022.

Kaiser, J., Skog, K. M., Baumann, K., Bertman, S. B., Brown, S. B., Brune, W. H., Crounse, J. D., De Gouw, J. A., Edgerton, E. S., Feiner, P. A., Goldstein, A. H., Koss, A., Misztal, P. K., Nguyen, T. B., Olson, K. F., St Clair, J. M., Teng, A. P., Toma, S., Wennberg, P. O., Wild, R. J., Zhang, L., and Keutsch, F. N.: Speciation of OH reactivity above the canopy of an isoprene-dominated forest, Atmos. Chem. Phys., 16, 9349–9359, https://doi.org/10.5194/acp-16-9349-2016, 2016.

Kanaya, Y., Cao, R., Kato, S., Miyakawa, Y., Kajii, Y., Tanimoto, H., Yokouchi, Y., Mochida, M.,

https://doi.org/10.5194/egusphere-2022-854
Preprint. Discussion started: 27 September 2022

Kawamura, K., and Akimoto, H.: Chemistry of OH and HO_2 radicals observed at Rishiri Island, Japan, in September 2003: Missing daytime sink of HO_2 and positive nighttime correlations with monoterpenes, J. Geophys. Res. Atmos., 112, 1–17, https://doi.org/10.1029/2006JD007987, 2007a.

Kanaya, Y., Cao, R., Akimoto, H., Fukuda, M., Komazaki, Y., Yokouchi, Y., Koike, M., Tanimoto, H., Takegawa, N., and Kondo, Y.: Urban photochemistry in central Tokyo: 1. Observed and modeled OH and HO_2 radical concentrations during the winter and summer of 2004, J. Geophys. Res., 112, D21312, https://doi.org/10.1029/2007JD008670, 2007b.

Kim, S., Wolfe, G. M., Mauldin, L., Cantrell, C., Guenther, A., Karl, T., Turnipseed, A., Greenberg, J., Hall, S. R., Ullmann, K., Apel, E., Hornbrook, R., Kajii, Y., Nakashima, Y., Keutsch, F. N., Digangi, J. P., Henry, S. B., Kaser, L., Schnitzhofer, R., Graus, M., Hansel, A., Zheng, W., and Flocke, F. F.: Evaluation of HO_x sources and cycling using measurement- constrained model calculations in a 2-methyl-3-butene-2-ol (MBO) and monoterpene (MT) dominated ecosystem, Atmos. Chem. Phys., 13, 2031–2044, https://doi.org/10.5194/acp-13-2031-2013, 2013.

Kukui, A., Ancellet, G., and Le Bras, G.: Chemical ionisation mass spectrometer for measurements of OH and Peroxy radical concentrations in moderately polluted atmospheres, J. Atmos. Chem., 61, 133–154, https://doi.org/10.1007/s10874-009-9130-9, 2008.

Kukui, A., Legrand, M., Preunkert, S., Frey, M. M., Loisil, R., Gil Roca, J., Jourdain, B., King, M. D., France, J. L., and Ancellet, G.: Measurements of oh and RO_2 radicals at Dome C, East Antarctica, Atmos. Chem. Phys., 14, 12373–12392, https://doi.org/10.5194/acp-14-12373-2014, 2014.

Kürten, A., Rondo, L., Ehrhart, S., Curtius, J., Ku, A., Rondo, L., Ehrhart, S., and Curtius, J.: Calibration of a chemical ionization mass spectrometer for the measurement of gaseous sulfuric acid, J. Phys. Chem. A, 116, 6375–6386, https://doi.org/10.1021/jp212123n, 2012.

Kuyper, B., Wingrove, H., Lesch, T., Labuschagne, C., Say, D., Martin, D., Young, D., Khan, M. A. H., O'Doherty, S., Davies-Coleman, M. T., and Shallcross, D. E.: Atmospheric Toluene and Benzene Mole Fractions at Cape Town and Cape Point and an Estimation of the Hydroxyl Radical Concentrations in the Air above the Cape Peninsula, South Africa, ACS Earth Sp. Chem., 4, 24–34, https://doi.org/10.1021/acsearthspacechem.9b00207, 2020.

Lelieveld, J., Butler, T. M., Crowley, J. N., Dillon, T. J., Fischer, H., Ganzeveld, L., Harder, H., Lawrence, M. G., Martinez, M., Taraborrelli, D., and Williams, J.: Atmospheric oxidation capacity

https://doi.org/10.5194/egusphere-2022-854
Preprint. Discussion started: 27 September 2022

sustained by a tropical forest, Nature, 452, 737–740, https://doi.org/10.1038/nature06870, 2008.

Lew, M. M., Rickly, P. S., Bottorff, B. P., Reidy, E., Sklaveniti, S., Léonardis, T., Locoge, N., Dusanter, S., Kundu, S., Wood, E., and Stevens, P. S.: OH and HO_2 radical chemistry in a midlatitude forest: measurements and model comparisons, Atmos. Chem. Phys., 20, 9209–9230, https://doi.org/10.5194/acp-20-9209-2020, 2020.

Li, Z., Xue, L., Yang, X., Zha, Q., Tham, Y. J., Yan, C., Louie, P. K. K., Luk, C. W. Y., Wang, T., and Wang, W.: Oxidizing capacity of the rural atmosphere in Hong Kong, Southern China, Sci. Total Environ., 612, 1114–1122, https://doi.org/10.1016/j.scitotenv.2017.08.310, 2018.

Liao, J., Huey, L. G., Tanner, D. J., Brough, N., Brooks, S., Dibb, J. E., Stutz, J., Thomas, J. L., Lefer, B., Haman, C., and Gorham, K.: Observations of hydroxyl and peroxy radicals and the impact of BrO at Summit, Greenland in 2007 and 2008, Atmos. Chem. Phys., 11, 8577–8591, https://doi.org/10.5194/acp-11-8577-2011, 2011.

Lu, K., Guo, S., Tan, Z., Wang, H., Shang, D., Liu, Y., Li, X., Wu, Z., Hu, M., and Zhang, Y.: Exploring atmospheric free-radical chemistry in China: The self-cleansing capacity and the formation of secondary air pollution, Natl. Sci. Rev., 6, 579–594, https://doi.org/10.1093/nsr/nwy073, 2019a.

Lu, K., Fuchs, H., Hofzumahaus, A., Tan, Z., Wang, H., Zhang, L., Schmitt, S. H., Rohrer, F., Bohn, B., Broch, S., Dong, H., Gkatzelis, G. I., Hohaus, T., Holland, F., Li, X., Liu, Y., Liu, Y., Ma, X., Novelli, A., Schlag, P., Shao, M., Wu, Y., Wu, Z., Zeng, L., Hu, M., Kiendler-Scharr, A., Wahner, A., and Zhang, Y.: Fast Photochemistry in Wintertime Haze: Consequences for Pollution Mitigation Strategies, Environ. Sci. Technol., 53, 10676–10684, https://doi.org/10.1021/acs.est.9b02422, 2019b.

Lu, K. D., Rohrer, F., Holland, F., Fuchs, H., Bohn, B., Brauers, T., Chang, C. C., Häseler, R., Hu, M., Kita, K., Kondo, Y., Li, X., Lou, S. R., Nehr, S., Shao, M., Zeng, L. M., Wahner, A., Zhang, Y. H., and Hofzumahaus, A.: Observation and modelling of OH and HO_2 concentrations in the Pearl River Delta 2006: A missing OH source in a VOC rich atmosphere, Atmos. Chem. Phys., 12, 1541–1569, https://doi.org/10.5194/acp-12-1541-2012, 2012.

Lu, K. D., Hofzumahaus, A., Holland, F., Bohn, B., Brauers, T., Fuchs, H., Hu, M., Häseler, R., Kita, K., Kondo, Y., Li, X., Lou, S. R., Oebel, A., Shao, M., Zeng, L. M., Wahner, A., Zhu, T., Zhang, Y. H., and Rohrer, F.: Missing OH source in a suburban environment near Beijing: Observed and modelled OH and HO_2 concentrations in summer 2006, Atmos. Chem. Phys., 13, 1057–1080,

https://doi.org/10.5194/egusphere-2022-854
Preprint. Discussion started: 27 September 2022

https://doi.org/10.5194/acp-13-1057-2013, 2013a.

Lu, Q., Zheng, J., Ye, S., Shen, X., Yuan, Z., and Yin, S.: Emission trends and source characteristics of SO_2, NO_x, PM10 and VOCs in the Pearl River Delta region from 2000 to 2009, Atmos. Environ., 76, 11–20, https://doi.org/10.1016/j.atmosenv.2012.10.062, 2013b.

M. Pugh, T. A., MacKenzie, A. R., Hewitt, C. N., Langford, B., Edwards, P. M., Furneaux, K. L., Heard, D. E., Hopkins, J. R., Jones, C. E., Karunaharan, A., Lee, J., Mills, G., Misztal, P., Moller, S., Monks, P. S., and Whalley, L. K.: Simulating atmospheric composition over a South-East Asian tropical rainforest: Performance of a chemistry box model, Atmos. Chem. Phys., 10, 279–298, https://doi.org/10.5194/acp-10-279-2010, 2010.

Ma, X., Tan, Z., Lu, K., Yang, X., Liu, Y., Li, S., Li, X., Chen, S., Novelli, A., Cho, C., Zeng, L., Wahner, A., and Zhang, Y.: Winter photochemistry in Beijing: Observation and model simulation of OH and HO2 radicals at an urban site, Sci. Total Environ., 685, 85–95, https://doi.org/10.1016/j.scitotenv.2019.05.329, 2019.

Mao, J., Jacob, D. J., Evans, M. J., Olson, J. R., Ren, X., Brune, W. H., St. Clair, J. M., Crounse, J. D., Spencer, K. M., Beaver, M. R., Wennberg, P. O., Cubison, M. J., Jimenez, J. L., Fried, A., Weibring, P., Walega, J. G., Hall, S. R., Weinheimer, A. J., Cohen, R. C., Chen, G., Crawford, J. H., McNaughton, C., Clarke, A. D., Jaeglé, L., Fisher, J. A., Yantosca, R. M., Le Sager, P., and Carouge, C.: Chemistry of hydrogen oxide radicals (HO_x) in the Arctic troposphere in spring, Atmos. Chem. Phys., 10, 5823–5838, https://doi.org/10.5194/acp-10-5823-2010, 2010.

Mao, J., Ren, X., Zhang, L., Van Duin, D. M., Cohen, R. C., Park, J. H., Goldstein, A. H., Paulot, F., Beaver, M. R., Crounse, J. D., Wennberg, P. O., Digangi, J. P., Henry, S. B., Keutsch, F. N., Park, C., Schade, G. W., Wolfe, G. M., Thornton, J. A., and Brune, W. H.: Insights into hydroxyl measurements and atmospheric oxidation in a California forest, Atmos. Chem. Phys., 12, 8009–8020, https://doi.org/10.5194/acp-12-8009-2012, 2012.

Mauldin, R., Kosciuch, E., Eisele, F., Huey, G., Tanner, D., Sjostedt, S., Blake, D., Chen, G., Crawford, J., and Davis, D.: South Pole Antarctica observations and modeling results: New insights on HO_x radical and sulfur chemistry, Atmos. Environ., 44, 572–581, https://doi.org/10.1016/j.atmosenv.2009.07.058, 2010.

Mauldin, R. L., Eisele, F. L., Kosciuch, E., Shetter, R., Lefer, B., Buhr, M., Chen, G., Wang, P., and

https://doi.org/10.5194/egusphere-2022-854
Preprint. Discussion started: 27 September 2022

Davis, D.: Measurements of OH, H_2SO_4 and MSA at the South Pole during ISCAT, Geophys. Res. Lett., 28, 3629–3632, 2001a.

Mauldin, R. L., Eisele, F. L., Cantrell, C. A., Kosciuch, E., Ridley, B. A., Lefer, B., Tanner, D. J., Nowak, J. B., Chen, G., Wang, L., Davis, D., Canttell, C. A., Kosciuch, E., Ridley, B. A., Tanner, D. J., Nowak, J. B., Chen, G., Wang, L., Davis, D., and Iris, I.: Measurements of OH aboard the NASA P-3 during PEM-Tropics B, J. Geophys. Res. Atmos., 106, 32657–32666, https://doi.org/10.1029/2000JD900832, 2001b.

Mauldin, R. L., Berndt, T., Sipilä, M., Paasonen, P., Petäjä, T., Kim, S., Kurtén, T., Stratmann, F., Kerminen, V. M., and Kulmala, M.: A new atmospherically relevant oxidant of sulphur dioxide, Nature, 488, 193–196, https://doi.org/10.1038/nature11278, 2012.

McKeen, S. A., Mount, G., Eisele, F., Williams, E., Harder, J., Goldan, P., Kuster, W., Liu, S. C., Baumann, K., Tanner, D., Fried, A., Sewell, S., Cantrell, C., and Shetter, R.: Photochemical modeling of hydroxyl and its relationship to other species during the Tropospheric OH Photochemistry Experiment, J. Geophys. Res. Atmos., 102, 6467–6493, https://doi.org/10.1029/96jd03322, 1997.

Novelli, A., Hens, K., Tatum Ernest, C., Kubistin, D., Regelin, E., Elste, T., Plass-Dülmer, C., Martinez, M., Lelieveld, J., and Harder, H.: Characterisation of an inlet pre-injector laser-induced fluorescence instrument for the measurement of atmospheric hydroxyl radicals, Atmos. Meas. Tech., 7, 3413–3430, https://doi.org/10.5194/amt-7-3413-2014, 2014a.

Novelli, A., Vereecken, L., Lelieveld, J., and Harder, H.: Direct observation of OH formation from stabilised Criegee intermediates, Phys. Chem. Chem. Phys., 16, 19941–19951, https://doi.org/10.1039/c4cp02719a, 2014b.

Novelli, A., Vereecken, L., Bohn, B., Dorn, H. P., Gkatzelis, G. I., Hofzumahaus, A., Holland, F., Reimer, D., Rohrer, F., Rosanka, S., Taraborrelli, D., Tillmann, R., Wegener, R., Yu, Z., Kiendler-Scharr, A., Wahner, A., and Fuchs, H.: Importance of isomerization reactions for OH radical regeneration from the photo-oxidation of isoprene investigated in the atmospheric simulation chamber SAPHIR, Atmos. Chem. Phys., 20, 3333–3355, https://doi.org/10.5194/acp-20-3333-2020, 2020.

Peeters, J. and Müller, J. F.: HO_x radical regeneration in isoprene oxidation via peroxy radical isomerisations. II: Experimental evidence and global impact, Phys. Chem. Chem. Phys., 12, 14227–14235, https://doi.org/10.1039/c0cp00811g, 2010.

https://doi.org/10.5194/egusphere-2022-854
Preprint. Discussion started: 27 September 2022

Peeters, J., Nguyen, T. L., and Vereecken, L.: HO_x radical regeneration in the oxidation of isoprene, Phys. Chem. Chem. Phys., 11, 5935–5939, https://doi.org/10.1039/b908511d, 2009.

Peeters, J., Müller, J. F., Stavrakou, T., and Nguyen, V. S.: Hydroxyl radical recycling in isoprene oxidation driven by hydrogen bonding and hydrogen tunneling: The upgraded LIM1 mechanism, J. Phys. Chem. A, 118, 8625–8643, https://doi.org/10.1021/jp5033146, 2014.

Peng, X., Wang, T., Wang, W., Ravishankara, A. R., George, C., Xia, M., Cai, M., Li, Q., Salvador, C. M., Lau, C., Lyu, X., Poon, C. N., Mellouki, A., Mu, Y., Hallquist, M., Saiz-lopez, A., Guo, H., Herrmann, H., Yu, C., Dai, J., Wang, Y., Wang, X., Yu, A., Leung, K., Lee, S., and Chen, J.: Photodissociation of particulate nitrate as a source of daytime tropospheric Cl_2, Nat. Commun., 13, 1–10, https://doi.org/10.1038/s41467-022-28383-9, 2022.

Petäjä, T., Mauldin, III, R. L., Kosciuch, E., McGrath, J., Nieminen, T., Paasonen, P., Boy, M., Adamov, A., Kotiaho, T., and Kulmala, M.: Sulfuric acid and OH concentrations in a boreal forest site, Atmos. Chem. Phys., 9, 7435–7448, https://doi.org/10.5194/acp-9-7435-2009, 2009.

Pu, W., Zou, Z., Wang, W., Tanner, D., Wang, Z., and Wang, T.: Development of a chemical ionization mass spectrometry system for measurement of atmospheric OH radical, Atmos. Meas. Tech. Discuss., 68, 1–12, https://doi.org/10.5194/amt-2020-252, 2020.

Ren, X., Harder, H., Martinez, M., Lesher, R. L., Oliger, A., Shirley, T., Adams, J., Simpas, J. B., and Brune, W. H.: HO_x concentrations and OH reactivity observations in New York City during PMTACS-NY2001, Atmos. Environ., 37, 3627–3637, https://doi.org/10.1016/S1352-2310(03)00460-6, 2003a.

Ren, X., Harder, H., Martinez, M., Lesher, R. L., Oliger, A., Simpas, J. B., Brune, W. H., Schwab, J. J., Demerjian, K. L., He, Y., Zhou, X., and Gao, H.: OH and HO_2 chemistry in the urban atmosphere of New York City, Atmos. Environ., 37, 3639–3651, https://doi.org/10.1016/S1352-2310(03)00459-X, 2003b.

Ren, X., Brune, W. H., Oliger, A., Metcalf, A. R., Simpas, J. B., Shirley, T., Schwab, J. J., Bai, C., Roychowdhury, U., Li, Y., Cai, C., Demerjian, K. L., He, Y., Zhou, X., Gao, H., and Hou, J.: OH, HO_2, and OH reactivity during the PMTACS-NY Whiteface Mountain 2002 campaign: Obervations and model comparison, J. Geophys. Res. Atmos., 111, 1–12, https://doi.org/10.1029/2005JD006126, 2006.

https://doi.org/10.5194/egusphere-2022-854
Preprint. Discussion started: 27 September 2022

Ren, X., van Duin, D., Cazorla, M., Chen, S., Mao, J., Zhang, L., Brune, W. H., Flynn, J. H., Grossberg, N., Lefer, B. L., Rappenglück, B., Wong, K. W., Tsai, C., Stutz, J., Dibb, J. E., Thomas Jobson, B., Luke, W. T., and Kelley, P.: Atmospheric oxidation chemistry and ozone production: Results from SHARP 2009 in Houston, Texas, J. Geophys. Res. Atmos., 118, 5770–5780, https://doi.org/10.1002/jgrd.50342, 2013.

Rohrer, F. and Berresheim, H.: Strong correlation between levels of tropospheric hydroxyl radicals and solar ultraviolet radiation, Nature, 442, 184–187, https://doi.org/10.1038/nature04924, 2006.

Rohrer, F., Lu, K., Hofzumahaus, A., Bohn, B., Brauers, T., Chang, C. C., Fuchs, H., Häseler, R., Holland, F., Hu, M., Kita, K., Kondo, Y., Li, X., Lou, S., Oebel, A., Shao, M., Zeng, L., Zhu, T., Zhang, Y., Wahner, A., Zeng, L., Zhang, Y., Wahner, A., Sinica, A., Univer-, S. J., Häseler, R., Holland, F., Hu, M., Kita, K., Kondo, Y., Li, X., Lou, S., Oebel, A., Shao, M., Zeng, L., Zhu, T., Zhang, Y., and Wahner, A.: Maximum efficiency in the hydroxyl-radical-based self-cleansing of the troposphere, Nat. Geosci., 7, 559–563, https://doi.org/10.1038/ngeo2199, 2014.

Saunders, S. M., Jenkin, M. E., Derwent, R. G., and Pilling, M. J.: Protocol for the development of the Master Chemical Mechanism, MCM v3 (Part A): tropospheric degradation of non-aromatic volatile organic compounds, Atmos. Chem. Phys., 3, 161–180, https://doi.org/10.5194/acp-3-161-2003, 2003.

Shirley, T. R., Brune, W. H., Ren, X., Mao, J., Lesher, R., Cardenas, B., Volkamer, R., Molina, L. T., Molina, M. J., Lamb, B., Velasco, E., Jobson, T., and Alexander, M.: Atmospheric oxidation in the Mexico City Metropolitan Area (MCMA) during April 2003, Atmos. Chem. Phys., 6, 2753–2765, https://doi.org/10.5194/acp-6-2753-2006, 2006.

Da Silva, G.: Hydroxyl radical regeneration in the photochemical oxidation of glyoxal: Kinetics and mechanism of the HC(O)CO + O_2 reaction, Phys. Chem. Chem. Phys., 12, 6698–6705, https://doi.org/10.1039/b927176g, 2010.

Sjostedt, S. J. J., Huey, L. G. G., Tanner, D. J. J., Peischl, J., Chen, G., Dibb, J. E. E., Lefer, B., Hutterli, M. A. A., Beyersdorf, A. J. J., Blake, N. J. J., Blake, D. R. R., Sueper, D., Ryerson, T., Burkhart, J., and Stohl, A.: Observations of hydroxyl and the sum of peroxy radicals at Summit, Greenland during summer 2003, Atmos. Environ., 41, 5122–5137, https://doi.org/10.1016/j.atmosenv.2006.06.065, 2007.

Slater, E. J., Whalley, L. K., Woodward-Massey, R., Ye, C., Lee, J. D., Squires, F. F. F., Hopkins, J.

https://doi.org/10.5194/egusphere-2022-854
Preprint. Discussion started: 27 September 2022

R., Dunmore, R. E., Shaw, M., Hamilton, J. F., Lewis, A. C. R., Crilley, L. R., Kramer, L., Bloss, W., Vu, T., Sun, Y., Xu, W., Yue, S., Ren, L., Joe, W., Nicholas Hewitt, C., Wang, X., Fu, P., Heard, D. E., Acton, W. J. F., Hewitt, C. N., Wang, X., Fu, P., and Heard, D. E.: Elevated levels of OH observed in haze events during wintertime in central Beijing, Atmos. Chem. Phys., 20, 14847–14871, https://doi.org/10.5194/acp-20-14847-2020, 2020.

Sommariva, R., Haggerstone, A.-L., Carpenter, L. J., Carslaw, N., Creasey, D. J., Heard, D. E., Lee, J. D., Lewis, A. C., Pilling, M. J., and Zádor, J.: OH and HO_2 chemistry in clean marine air during SOAPEX-2, Atmos. Chem. Phys., 4, 839–856, https://doi.org/10.5194/acp-4-839-2004, 2004.

Stone, D., Evans, M. J., Edwards, P. M., Commane, R., Ingham, T., Rickard, A. R., Brookes, D. M., Hopkins, J., Leigh, R. J., Lewis, A. C., Monks, P. S., Oram, D., Reeves, C. E., Stewart, D., and Heard, D. E.: Isoprene oxidation mechanisms: measurements and modelling of OH and HO_2 over a South-East Asian tropical rainforest during the OP3 field campaign, Atmos. Chem. Phys., 11, 6749–6771, https://doi.org/10.5194/acp-11-6749-2011, 2011.

Stone, D., Whalley, L. K., and Heard, D. E.: Tropospheric OH and HO_2 radicals: Field measurements and model comparisons, Chem. Soc. Rev., 41, 6348–6404, https://doi.org/10.1039/c2cs35140d, 2012.

Tan, D., Faloona, I., Simpas, J. B., Brune, W., Shepson, P. B., Couch, T. L., Sumner, A. L., Carroll, M. A., Thornberry, T., Apel, E., Riemer, D., and Stockwell, W.: HO_x budgets in a deciduous forest: Results from the PROPHET summer 1998 campaign, J. Geophys. Res. Atmos., 106, 24407–24427, https://doi.org/10.1029/2001JD900016, 2001.

Tan, Z., Fuchs, H., Lu, K., Hofzumahaus, A., Bohn, B., Broch, S., Dong, H., Gomm, S., Häseler, R., He, L., Holland, F., Li, X., Liu, Y., Lu, S., Rohrer, F., Shao, M., Wang, B., Wang, M., Wu, Y., Zeng, L., Zhang, Y., Wahner, A., and Zhang, Y.: Radical chemistry at a rural site (Wangdu) in the North China Plain: Observation and model calculations of OH, HO_2 and RO_2 radicals, Atmos. Chem. Phys., 17, 663–690, https://doi.org/10.5194/acp-17-663-2017, 2017.

Tan, Z., Rohrer, F., Lu, K., Ma, X., Bohn, B., Broch, S., Dong, H., Fuchs, H., Gkatzelis, G. I., Hofzumahaus, A., Holland, F., Li, X., Liu, Y., Liu, Y., Novelli, A., Shao, M., Wang, H., Wu, Y., Zeng, L., Hu, M., Kiendler-Scharr, A., Wahner, A., and Zhang, Y.: Wintertime photochemistry in Beijing: Observations of ROx radical concentrations in the North China Plain during the BEST-ONE campaign, Atmos. Chem. Phys., 18, 12391–12411, https://doi.org/10.5194/acp-18-12391-2018, 2018.

https://doi.org/10.5194/egusphere-2022-854
Preprint. Discussion started: 27 September 2022

Tan, Z., Lu, K., Hofzumahaus, A., Fuchs, H., Bohn, B., Holland, F., Liu, Y., Rohrer, F., Shao, M., Sun, K., Wu, Y., Zeng, L., Zhang, Y., Zou, Q., Kiendler-Scharr, A., Wahner, A., and Zhang, Y.: Experimental budgets of OH, HO_2, and RO_2 radicals and implications for ozone formation in the Pearl River Delta in China 2014, Atmos. Chem. Phys., 19, 7129–7150, https://doi.org/10.5194/acp-19-7129-2019, 2019.

Tanner, D. J. and Eisele, F. L.: Present OH measurement limits and associated uncertainties, J. Geophys. Res., 100, 2883, https://doi.org/10.1029/94JD02609, 1995.

Tanner, D. J., Jefferson, A., and Eisele, F. L.: Selected ion chemical ionization mass spectrometric measurement of OH, J. Geophys. Res. Atmos., 102, 6415–6425, https://doi.org/10.1029/96jd03919, 1997.

Tang, J. H., Chan, L. Y., Chan, C. Y., Li, Y. S., Chang, C. C., Wang, X. M., Zou, S. C., Barletta, B., Blake, D. R., and Wu, D.: Implications of changing urban and rural emissions on non-methane hydrocarbons in the Pearl River Delta region of China, Atmos. Environ., 42, 3780–3794, https://doi.org/10.1016/j.atmosenv.2007.12.069, 2008.

Thames, A. B., Brune, W. H., Miller, D. O., Allen, H. M., Apel, E. C., Blake, D. R., Paul Bui, T., Commane, R., Crounse, J. D., Daube, B. C., Diskin, G. S., Digangi, J. P., Elkins, J. W., Hall, S. R., Hanisco, T. F., Hannun, R. A., Hintsa, E., Hornbrook, R. S., Kim, M. J., McKain, K., Moore, F. L., Nicely, J. M., Peischl, J., Ryerson, T. B., St. Clair, J. M., Sweeney, C., Teng, A., Thompson, C. R., Ullmann, K., Wennberg, P. O., and Wolfe, G. M.: Missing OH reactivity in the global marine boundary layer, Atmos. Chem. Phys., 20, 4013–4029, https://doi.org/10.5194/acp-20-4013-2020, 2020.

Volz-Thomas, A., Pätz, H. W., Houben, N., Konrad, S., Mihelcic, D., Klüpfel, T., and Perner, D.: Inorganic trace gases and peroxy radicals during BERLIOZ at Pabstthum: An investigation of the photostationary state of NO_x and O_3, J. Geophys. Res. Atmos., 108, 1–15, https://doi.org/10.1029/2001jd001255, 2003a.

Volz-Thomas, A., Geiss, H., Hofzumahaus, A., and Becker, K. H.: Introduction to special section: Photochemistry experiment in BERLIOZ, J. Geophys. Res. Atmos., 108, https://doi.org/10.1029/2001jd002029, 2003b.

Wang, F., Hu, R., Chen, H., Xie, P., Wang, Y., Li, Z., Jin, H., Liu, J., and Liu, W.: Development of a

https://doi.org/10.5194/egusphere-2022-854
Preprint. Discussion started: 27 September 2022

field system for measurement of tropospheric OH radical using laser-induced fluorescence technique, Opt. Express, 27, A419, https://doi.org/10.1364/oe.27.00a419, 2019a.

Wang, T., Dai, J., Lam, K. S., Nan Poon, C., and Brasseur, G. P.: Twenty-Five Years of Lower Tropospheric Ozone Observations in Tropical East Asia: The Influence of Emissions and Weather Patterns, Geophys. Res. Lett., 46, 11463–11470, https://doi.org/10.1029/2019GL084459, 2019b.

Wang, Y., Hu, R., Xie, P., Chen, H., Wang, F., Liu, X., Liu, J. G., and Liu, W.: Measurement of tropospheric HO_2 radical using fluorescence assay by gas expansion with low interferences, J. Environ. Sci. (China), 99, 40–50, https://doi.org/10.1016/j.jes.2020.06.010, 2021.

Wang, Y. Q.: MeteoInfo: GIS software for meteorological data visualization and analysis, Meteorol. Appl., 21, 360–368, https://doi.org/10.1002/met.1345, 2014.

Wang, Y. Q.: An Open Source Software Suite for Multi-Dimensional Meteorological Data Computation and Visualisation, J. Open Res. Softw., 7, 1–9, https://doi.org/10.5334/jors.267, 2019.

Whalley, L. K., Edwards, P. M., Furneaux, K. L., Goddard, A., Ingham, T., Evans, M. J., Stone, D., Hopkins, J. R., Jones, C. E., Karunaharan, A., Lee, J. D., Lewis, A. C., Monks, P. S., Moller, S. J., and Heard, D. E.: Quantifying the magnitude of a missing hydroxyl radical source in a tropical rainforest, Atmos. Chem. Phys., 11, 7223–7233, https://doi.org/10.5194/acp-11-7223-2011, 2011.

Whalley, L. K., Stone, D., Dunmore, R., Hamilton, J., Hopkins, J. R., Lee, J. D., Lewis, A. C., Williams, P., Kleffmann, J., Laufs, S., Woodward-Massey, R., and Heard, D. E.: Understanding in situ ozone production in the summertime through radical observations and modelling studies during the Clean air for London project (ClearfLo), Atmos. Chem. Phys., 18, 2547–2571, https://doi.org/10.5194/acp-18-2547-2018, 2018.

Whalley, L. K., Slater, E. J., Woodward-Massey, R., Ye, C., Lee, J. D., Squires, F., Hopkins, J. R., Dunmore, R. E., Shaw, M., Hamilton, J. F., Lewis, A. C., Mehra, A., Worrall, S. D., Bacak, A., Bannan, T. J., Coe, H., Percival, C. J., Ouyang, B., Jones, R. L., Crilley, L. R., Kramer, L. J., Bloss, W. J., Vu, T., Kotthaus, S., Grimmond, S., Sun, Y., Xu, W., Yue, S., Ren, L., Joe, W., Nicholas Hewitt, C., Wang, X., Fu, P., and Heard, D. E.: Evaluating the sensitivity of radical chemistry and ozone formation to ambient VOCs and NO_x in Beijing, Atmos. Chem. Phys., 21, 2125–2147, https://doi.org/10.5194/acp-21-2125-2021, 2021.

Wolfe, G. M., Cantrell, C., Kim, S., Mauldin, R. L., Karl, T., Harley, P., Turnipseed, A., Zheng, W.,

https://doi.org/10.5194/egusphere-2022-854
Preprint. Discussion started: 27 September 2022

Flocke, F., Apel, E. C., Hornbrook, R. S., Hall, S. R., Ullmann, K., Henry, S. B., Digangi, J. P., Boyle, E. S., Kaser, L., Schnitzhofer, R., Hansel, A., Graus, M., Nakashima, Y., Kajii, Y., Guenther, A., and Keutsch, F. N.: Missing peroxy radical sources within a summertime ponderosa pine forest, Atmos. Chem. Phys., 14, 4715–4732, https://doi.org/10.5194/acp-14-4715-2014, 2014.

Wolfe, G. M., Marvin, M. R., Roberts, S. J., Travis, K. R., and Liao, J.: The framework for 0-D atmospheric modeling (F0AM) v3.1, Geosci. Model Dev., 9, 3309–3319, https://doi.org/10.5194/gmd-9-3309-2016, 2016.

Woodward-Massey, R., Slater, E. J., Alen, J., Ingham, T., Ingham, T., Cryer, D. D. R., Stimpson, L. M., Ye, C., Seakins, P. W., Whalley, L. K., Whalley, L. K., Heard, D. E., Ingham, T., Cryer, D. D. R., Stimpson, L. M., Ye, C., Seakins, P. W., Whalley, L. K., Whalley, L. K., and Heard, D. E.: Implementation of a chemical background method for atmospheric OH measurements by laser-induced fluorescence: characterisation and observations from the UK and China, Atmos. Meas. Tech., 13, 3119–3146, https://doi.org/10.5194/amt-13-3119-2020, 2020.

Xiao, Y., Jacob, D. J., and Turquety, S.: Atmospheric acetylene and its relationship with CO as an indicator of air mass age, J. Geophys. Res. Atmos., 112, 1–14, https://doi.org/10.1029/2006JD008268, 2007.

Yang, Y., Shao, M., Wang, X., Nölscher, A. C., Kessel, S., Guenther, A., and Williams, J.: Towards a quantitative understanding of total OH reactivity: A review, Atmos. Environ., 134, 147–161, https://doi.org/10.1016/j.atmosenv.2016.03.010, 2016.

Yao, T., Fung, J. C. H., Ma, H., Lau, A. K. H., Chan, P. W., Yu, J. Z., and Xue, J.: Enhancement in secondary particulate matter production due to mountain trapping, Atmos. Res., 147–148, 227–236, https://doi.org/10.1016/j.atmosres.2014.05.007, 2014.

Zhang, G., Hu, R., Xie, P., Lu, K., Lou, S., Liu, X., Li, X., Wang, F., Wang, Y., Yang, X., Cai, H., Wang, Y., and Liu, W.: Intercomparison of OH radical measurement in a complex atmosphere in Chengdu, China, Sci. Total Environ., 838, 155924, https://doi.org/10.1016/j.scitotenv.2022.155924, 2022a.

Zhang, G., Hu, R., Xie, P., Lou, S., Wang, F., Wang, Y., Qin, M., Li, X., Liu, X., Wang, Y., and Liu, W.: Observation and simulation of HO_x radicals in an urban area in Shanghai, China, Sci. Total Environ., 810, 152275, https://doi.org/10.1016/j.scitotenv.2021.152275, 2022b.

https://doi.org/10.5194/egusphere-2022-854
Preprint. Discussion started: 27 September 2022

Zhang, M., Akimoto, H., and Uno, I.: A three-dimensional simulation of HO_x concentrations over East Asia during TRACE-P, J. Atmos. Chem., 54, 233–254, https://doi.org/10.1007/s10874-006-9015-0, 2006.

https://doi.org/10.5194/egusphere-2022-854
Preprint. Discussion started: 27 September 2022

Figures and Tables

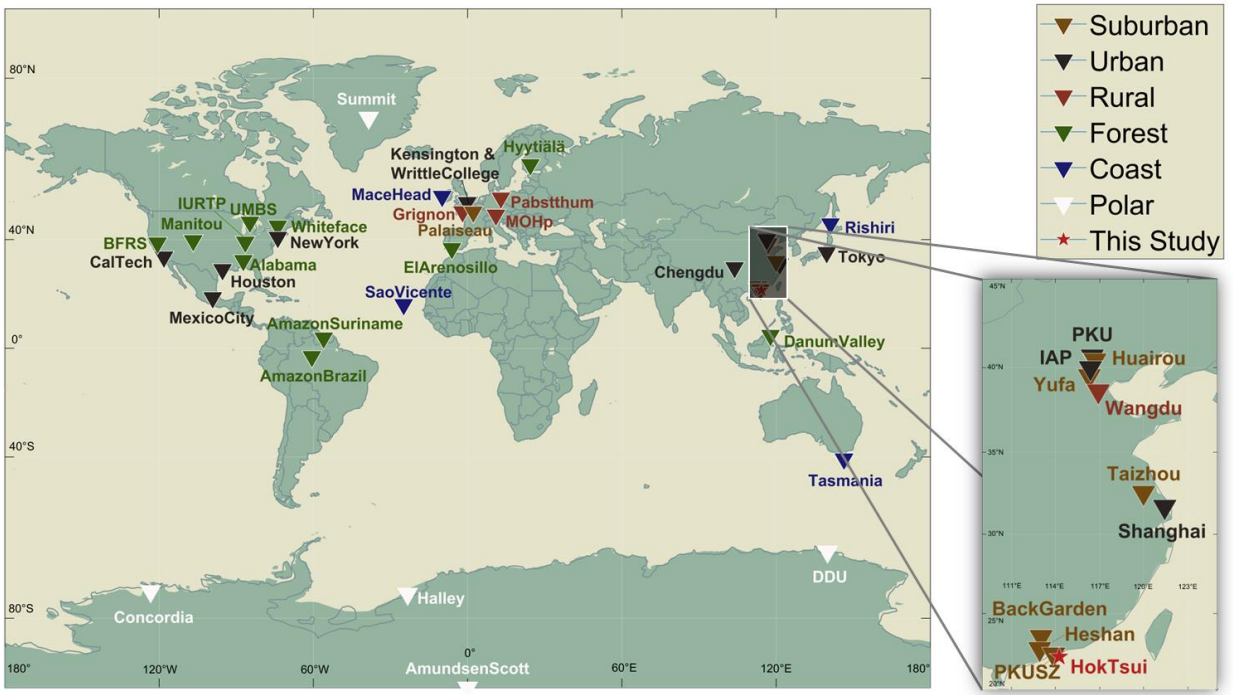

Figure 1. OH measurements gathered around the world to date.

Table 1. Summary of studies reporting OH and HO_2 measurements and comparing them with model predictions (refer to Figure 1 for site locations)

Comparison results (OH only)	Reference	Time	Location in Figure 1	Site types	Measurement notes	OH conc. 10^6 cm^{-3}	HO_2 conc. 10^8 cm^{-3}	Ratio notes	OH $R_{S/O}$	HO_2 $R_{S/O}$	Other references targeting the same site
Overprediction	(Berresheim, 2002)	June–July 1999	MaceHead	Coast	Mean (All) Peaks (Mean Clean) Peaks (Pollution)	0.12 2.5 18 & 12	N/A	Mean (17 June, Coastal) Mean (30 July, Continental)	2 ~1	N/A	(Carslaw et al., 1999); (Berresheim et al., 2013), 2014
Overprediction	(Sommariva et al., 2004); (Creasey et al., 2003);	Jan–Feb 1999	Tasmania	Coast	Mean (Peaks) Peaks (Range)	3.5 2 to 5.5	2 1 to 2.5	Mean (7–8 Feb) Mean (15–16 Feb)	~1.11 ~1.32	N/A ~2	N/A
Overprediction	(Kanaya et al., 2007a)	September 2003	Rishiri	Island Coast	Peaks (Mean)	2.7	1.45	OH rectified by constrained HO_2	1.35	1.89	N/A
Overprediction	Mauldin et al., 2010	Nov–Jan 2003-04	AmundsenScott	Antarctica	Mean (Range)	1.5 to 2.5	N/A	Mean	~2	N/A	Mauldin, Eisele, Kosciuch, et al., 2001
Overprediction	(Kukui et al., 2014)	Dec–Jan 2011-2012	Concordia	Antarctica	Mean (All) Peaks (Mean) Mean (range)	3.1 5.2 0.3 to 7.5	0.99* 1.7* 0.1 to 2*	Mean (w/PSS HONO) Mean (w/measured HONO)	0.72 2.19	1.02* 1.84*	N/A
Overprediction	(Dusanter et al., 2009a); a(O), b (M)	March 2006	MexicoCity	Urban	Peaks (Range) Peaks (Mean)	2 to 15 4.6	0.56 to 4.5 1.9	Mean (13:00 w/o glyoxal) Mean (Morning, polluted) Mean (11:00–14:30) Mean (After 14:30)	2.4 ~0.5 to ~1 1.7 ~1	1.5 0.2 to ~1 ~1 ~1	N/A
Overprediction	(Bloss et al., 2007)	Jan–Feb 2005	Halley	Polar	Mean (All) Peak (Mean)	0.39 0.79	2.04 4.03	Peak (S1: Conventional) Peak (S2: S1 + halogen oxides) Peak (S3: S2 + possible VOCs)	0.67 1.64 1.27	N/A	N/A
Overprediction	(Holland et al., 2003)	Jul–Aug 1998	Pabstthum	Rural	Peaks (Range)	6 to 8	5 to 7.4	Mean (Low NO_x)	2	1.4	N/A
Overprediction	(Whalley et al., 2018)	Jul–Aug 2012	Kensington	Urban	Mean (Noon; S-W air) Mean (Noon; E, polluted air)	~2.2 ~3	~0.2 ~0.5	Mean (Air mass: South-westerly) Mean (Air mass: Easterly, polluted)	1.25 2	~4 10	N/A
Overprediction	(Griffith et al., 2016)	May–June 2010	CalNexLA	Urban	Peaks (Range) Peaks (Weekdays) Peaks (Weekend)	1.5 to 9 ~4 ~5	0.8* to 10* ~3* ~8*	Mean (Weekend) Mean (Weekday)	1.43 1	0.77* 0.33*	(Volz-Thomas et al., 2003b); (Volz-Thomas et al., 2003a)

https://doi.org/10.5194/egusphere-2022-854
Preprint. Discussion started: 27 September 2022

Table 1. Continued

Comparison results (OH only)	Reference	Time	Location in Figure 1	Site types	Measurement notes	OH conc. 10^6 cm^{-3}	HO_2 conc. 10^8 cm^{-3}	Ratio notes	**OH $R_{S/O}$**	**HO_2 $R_{S/O}$**	Other references targeting the same site
Underprediction	(Hofzumahaus et al., 2009); (Lu et al., 2012)	July 2006	BackGarden	Rural	Peaks (Mean)	15	15	Mean (Range, NO < 1 ppb) Mean (Lu et al., 2012)	0.2 to 0.33 0.5	N/A	N/A
Underprediction	(Whalley et al., 2011)	Apr–May 2008	DanumValley	Rainforest	Peaks (Mean)	2.5	3	w/C_5H_8 recycling mechanism (Peeters et al,. 2009)	~0.63	~0.5	(M. Pugh et al., 2010)
Underprediction	(Liao et al., 2011)	May–June 2007 Jun–Jul 2008	Summit	Polar	Mean (2007 spring) Mean (2008 summer)	3.0 4.1	2.7* 4.2*	2007 spring w/o BrO & w BrO 2008 summer w/o BrO & w BrO	0.72 0.78 0.54 0.56	0.87 0.96	(Sjostedt et al., 2007)
Underprediction	(Wolfe et al., 2014)	Aug 2010	Manitou	Forest	Peaks (Range)	3 to 10	24.6 to 44.3	Peak	~0.625	0.33	(Kim et al., 2013)
Underprediction	(Tan et al., 2019)	Oct–Nov 2014	Heshan	Suburban	Peaks (Mean)	4.5	3	Budget analysis only	N/A	1	N/A
Underprediction	(Griffith et al., 2013)	Jul–Aug 2008 Jul–Aug 2009	UMBS	Forest	Peak (Mean, 2008) Peak (Mean, 2009)	~3.3 ~1.6	~7 ~4.8	Mean (2008) Mean (2008 w/ISOP mechanisms) Mean (2009) Mean (2009 w/ISOP mechanisms)	~0.4 0.9	~0.57 ~1.3 ~0.6 ~1.5	N/A
Underprediction	K.D. Lu et al., 2013	Sept 2006	Yufa	Urban	Peaks (Range) Peaks (Mean)	4 to 17 ~7	2 to 24 ~1.5	Mean (NO < 0.1 ppb) Mean (NO > 1 ppb)	0.38 ~1	~1 ~1	N/A
Underprediction	(Mao et al., 2012)	Jun–Jul 2009	BFRS	Forest	Peaks (Mean w/ interference) Peaks (Mean w/o interference)	~4.5 ~1.8	N/A	Mean (w/ interference) Mean (w/o interference)	0.32 0.71	N/A	N/A
Underprediction	(Tan et al., 2017) (Lu et al., 2019b)	Summer 2014	Wangdu	Rural	Peaks (Range noontime)	5 to 15	3 to 14	Mean (NO > 0.3 ppb) Mean (NO < 0.3 ppb, afternoon)	~1 0.5	10 (NO > 4 ppb) N/A	N/A
Underprediction	(Lew et al., 2020)	Jul 2015	IURTP	Forest	Peaks (Mean)	4	10	Mean (Daytime) Mean (Evening and morning)	0.83 0.50	1.10 to 1.32	N/A
Underprediction	(Lelieveld et al., 2008)	Oct 2005	AmazonSuriname	Forest (Flight)	Mean (Forest boundary) Mean (Forest free troposphere) Mean (Atlantic boundary) Mean (Atlantic free troposphere)	5.6 8.2 9.0 10.1	10.5 4.9 6.7 5.5	Mean (w/MIM: Mainz ISOP mechanism) Mean (w/MIM2+: extra 40% to 80% OH recycle)	0.1 to 0.2 ~1	N/A	N/A

Table 1. Continued

Comparison results (OH only)	Reference	Time	Location in Figure 1	Site types	Measurement notes	OH conc. 10^6 cm^{-3}	HO_2 conc. 10^8 cm^{-3}	Ratio notes	**OH $R_{S/O}$**	**HO_2 $R_{S/O}$**	Other reference targeting the same site
Good match	(Ren et al., 2003a); a(O), b(M)	Jun–Aug 2001	NewYork	Urban	Peaks (Range) Peaks (Mean)	2 to 20 7	0.5 to 6 1	Mean	0.91	0.81	N/A
Good match	(Ren et al., 2006)	Jul–Aug 2002	Whiteface	Forest	Peaks (Mean)	2.6	4.9	Mean	1.22	0.83	N/A
Good match	(Kanaya et al., 2007b)	Jan–Feb & Jul–Aug 2004	Tokyo	Urban	Peaks (Mean, winter) Peaks (Mean, summer)	1.5 6.3	0.27 1.4	Peaks (Mean, winter) Peaks (Mean, summer)	0.99 0.81	0.71 1.22	N/A
Good match	(Feiner et al., 2016); (Kaiser et al., 2016)	Jun–Jul 2013	Alabama	Forest	Peaks (Mean)	1	6.64	Peaks (Mean)	~1	~1	N/A
Good match	(Jeong et al., 2022)	Feb–Mar 2014	AmazonBrazil	Forest	Peaks (Mean 10:00-15:00) Peaks (Range)	1 ~1 to ~2.8	N/A	Mean	1	N/A	N/A
Good match	(Hens et al., 2014)	Summer 2010	Hyytiälä	Forest	Mean (Above-Canopy) Mean (Ground)	3.5 ~1.8 to ~1.2	N/A	Mean	1	0.3	(Petäjä et al., 2009); (Novelli et al., 2014b)
Good match	(Emmerson et al., 2007)	Jul–Aug 2003	WrittleCollege	Urban	Peaks (Range)	1.2 to 7.5	0.16 to 3.3	Mean	1.24	1.07	N/A
Good match	(Ren et al., 2013)	Apr–May 2009	Houston	Urban	Peak (Mean)	~8.8	~6.2	Mean	0.9	1.22	(Mao et al., 2010); (Chen et al., 2010)
Good match	(Ma et al., 2019)	Nov–Dec 2017	PKU	Urban	Peaks (Mean clean) Peaks (Mean polluted)	2 1.5	0.4 0.3	Mean (clean) Mean (polluted)	~1 ~0.66	~0.66 0.08	N/A
Good match with missing source	(Whalley et al., 2021)	Summer 2017	IAP	Urban	Peak (All)	28	10	Mean (NO < 1 ppb)	~1	1.83	(Slater et al., 2020)
Good match with underpredicted HO_2	(Zhang et al., 2022b)	Nov–Dec 2019	Shanghai	Urban	Peaks (Mean)	2.7	0.8	N/A	N/A	N/A	N/A
No comparison	(Kukui et al., 2008)	June–July 2007	Grignon	Suburban	Peak (July 6)	~23	~2	N/A	N/A	N/A	N/A
No comparison	(Wang et al., 2021)	Oct–Nov 2018	PKUSZ	Suburban	Peaks (Mean)	5.3	4.2	N/A	N/A	N/A	(Wang et al., 2019a)
No comparison	(Rohrer and Berresheim, 2006)	1999–2003	MOHp	Rural	Mean (All)	1.97	N/A	N/A	N/A	N/A	(Handisides et al., 2003); (Novelli et al., 2014b)

https://doi.org/10.5194/egusphere-2022-854
Preprint. Discussion started: 27 September 2022

No comparison	(Zhang et al., 2022a)	Aug–Sept 2019	Chengdu	Urban	Peaks (Range, PKU-LIF) Peaks (Range, AIOFM-LIF)	1.6 to 15 2.1 to 15.9	N/A	N/A	N/A	N/A	N/A

Notes

ISOP: Isoprene

AIOFM: Laser- induced fluorescence instrument by the Anhui Institute of Optics Fine Mechanics, Chinese Academy of Sciences

Mean: Campaign average concentration or ratio

Peak: Campaign maximum concentration or ratio

Peaks (Mean): Maximum concentration or ratio for the averaged diurnal or averaged cases

Mean (Range): Daily average concentration or ratio range for the campaign or cases

Peaks (Range): Maximum concentration or ratio range for the campaign or cases

w/ and w/o: Considered or did not consider the specific mechanism, species, or interference

~: The result is based on the figure or description, and the exact number is not mentioned in the article

N/A: Not available in the article

*: The HO_2 result includes some RO_2 species.

https://doi.org/10.5194/egusphere-2022-854
Preprint. Discussion started: 27 September 2022

https://doi.org/10.5194/egusphere-2022-854
Preprint. Discussion started: 27 September 2022

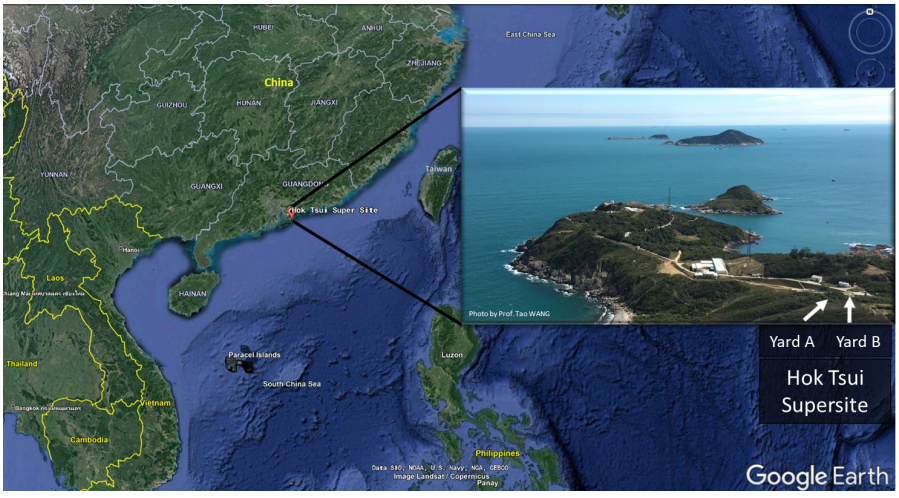

Figure 2. The location of the Hok Tsui Air Monitoring Supersite in Hong Kong, South China. The map is from © Google Earth.

https://doi.org/10.5194/egusphere-2022-854
Preprint. Discussion started: 27 September 2022

Table 2. Measuring instruments and measured species in the field campaign

Species	Instruments	Time resolution	Detection limit
OH	Nitrate-quadrupole chemical ionization mass spectrometer (CIMS)	10 s	Lab: 1.5×10^5 cm^{-3} Daytime: 1×10^6 cm^{-3}
NO, NO_2	Chemiluminescence/photolytic converter (Thermo, Model 42i)	1 min	0.06 ppb
Ozone	Ozone analyser, model 49i, Thermo Scientific	1 min	0.5 ppb
J_{NO2}	Filter radiometer, Metcon	1 min	4×10^{-5} s^{-1}
HONO	Iodide-ToF-CIMS, Aerodyne Inc	1 s	0.2 ppt
Particle number size distribution	Scanning mobility particle sizer (SMPS), TSI	5 mins	1 particle cm^{-3}
VOCs	Gas chromatograph system (GC-MS/FID; GC955 Series 611/811, Syntech Spectras)	1 hour	~10 ppt
	Proton-transfer-reaction mass spectrometry (PTR-MS; PTR-QMS 500, IONICON Analytik, Austria)	5 mins	20 ppt
OVOCs	High-performance liquid chromatography (HPLC); PTR-ToF-MS, IONICON Analytic;	1 s	~10 ppt

https://doi.org/10.5194/egusphere-2022-854
Preprint. Discussion started: 27 September 2022

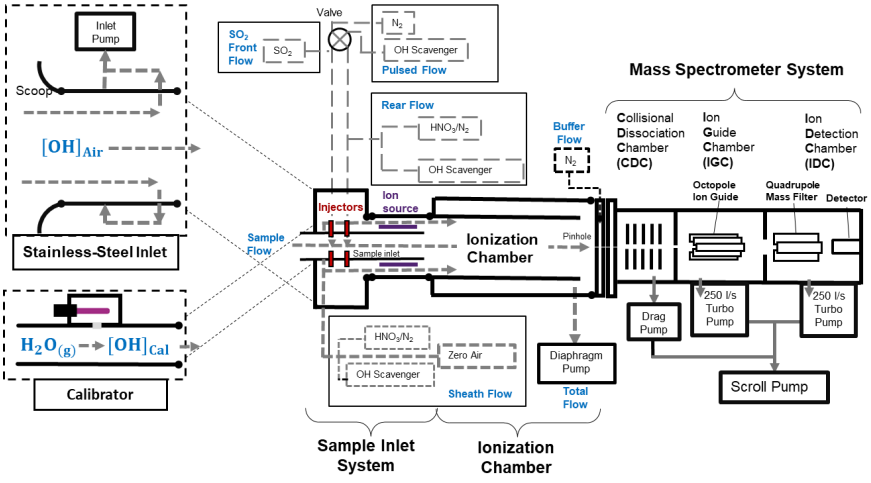

Figure 3. Schematics of the CIMS system which consists of a stainless-steel inlet, a sample inlet, an ionization chamber, a mass spectrometer system, and a calibration unit. The CIMS measures the ambient OH concentration when connecting to the stainless-steel inlet whereas, during calibration, the calibration unit is connected to the CIMS instead. Details of the CIMS setup and calibration can be found in Section 2.2.

https://doi.org/10.5194/egusphere-2022-854
Preprint. Discussion started: 27 September 2022

Table 3. Technical specifications of the OH-CIMS

Flow position	**Gas**	**Flow rates (sccm)**	**Specification for measurement**	
Front injectors	SO_2 (0.9%)	5	Sample flow [SO_2] (ppm)	12
	NO (0.9%)	0	Sample flow [NO] (ppm)	0
Pulse valve	C_3F_6 (99.9%)	2	Elimination rate	95%
	N_2	2	Switching time (min)	2
Rear injectors	C_3F_6 (99.9%)	2	Reaction time (ms)	47
	HNO3	10	Sample flow [C_3F_6] (ppm)	1072
Sheath flow	C_3F_6 (99.9%)	2	Sheath flow [C_3F_6] (ppm)	159
	HNO_3	10	Detection Limit in lab ($\times10^5$ cm^{-3})	1.5
	Zero air	126,000	Sheath flow speed (cm/s)	25
Buffer	N_2	440	Reynolds number in ionization chamber	> 4000
Total flow		168,000	Sample flow speed (cm/s)	55
Sample flow		3727	Stainless-steel inlet flow speed (m/s)	5
Calibration flow		10,000	Calibration flow speed (cm/s)	65
Calibration factors for OH with $N^{18}O_3^-$ as the reagent ion $\times10^{-8}$ ($(OH{\cdot}cm^{-3})$/Hz)				1.21
Detection limit for OH measurement over the whole campaign ($\times10^5$ cm^{-3}) (2σ)			Daytime	10
			Nighttime	7.7
Uncertainties for OH measurement				44%

https://doi.org/10.5194/egusphere-2022-854
Preprint. Discussion started: 27 September 2022

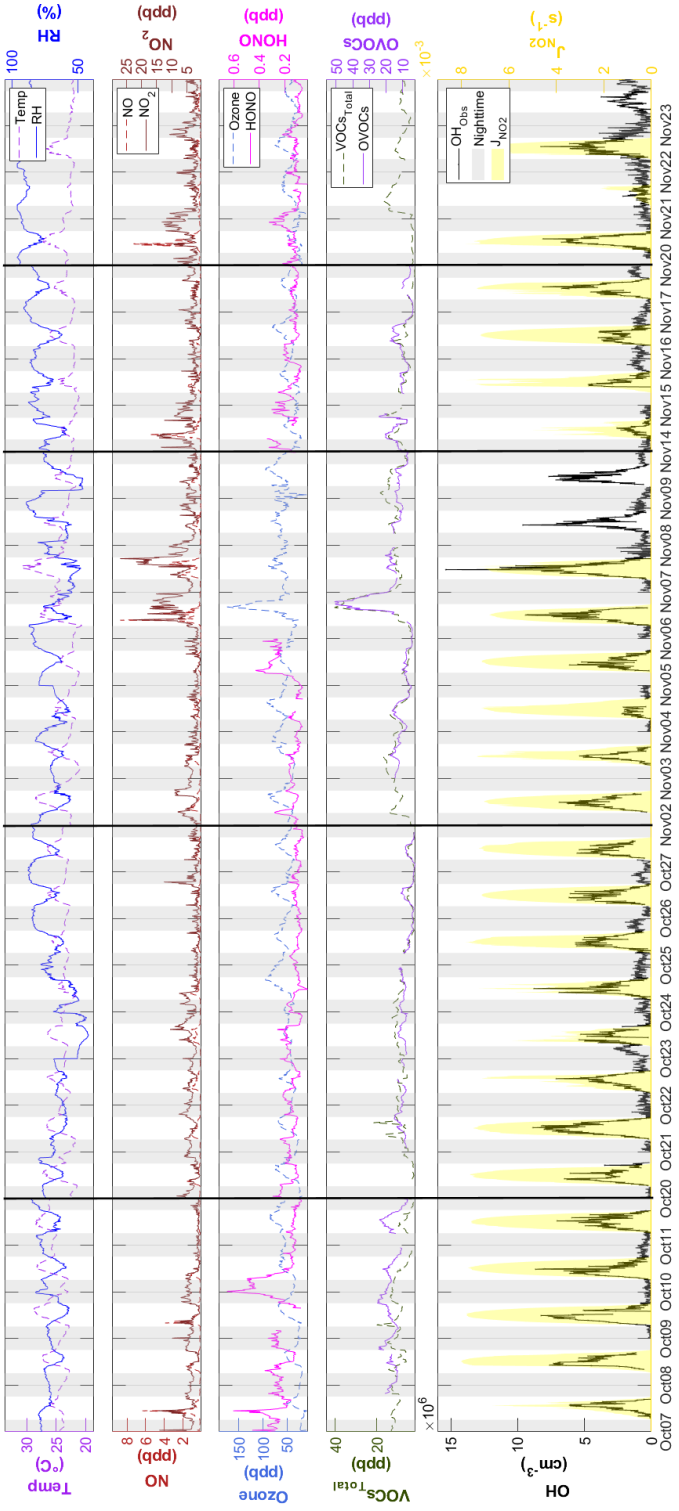

Figure 4. Time series of OH between 7 October and 23 November with measured weather conditions (temperature and RH), OH primary sources (ozone and HONO), NO_x (NO and NO_2), organic compounds (total VOCs and OVOCs), and photolysis frequency (J_{NO2}). All measurement data shown are 10 min averages. The black lines separate the non-continuous days during measurement. The grey shaded area denotes nighttime.

https://doi.org/10.5194/egusphere-2022-854
Preprint. Discussion started: 27 September 2022

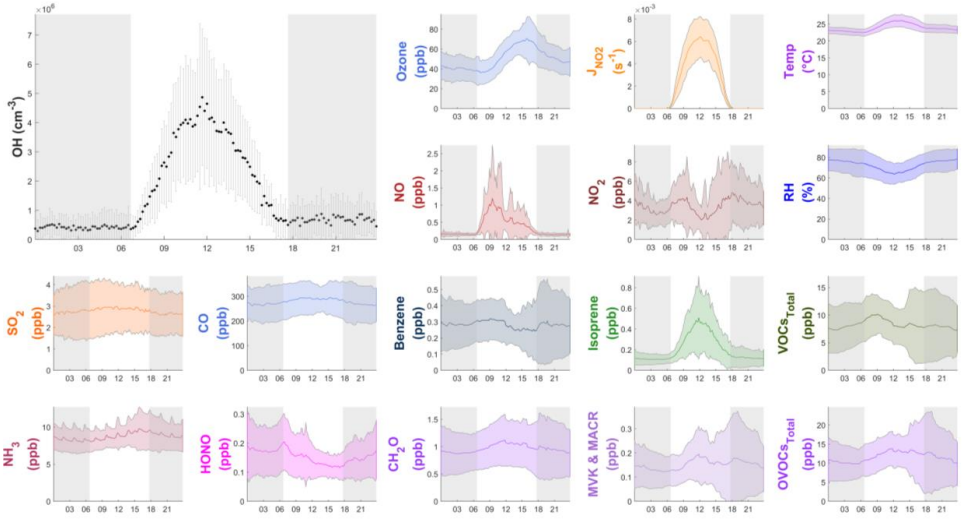

Figure 5. Diurnal profiles of the average (±1σ) concentrations of OH, other chemical species, and meteorological parameters (*T*, RH, J_{NO2}) during the field campaign. The grey shaded area denotes nighttime.

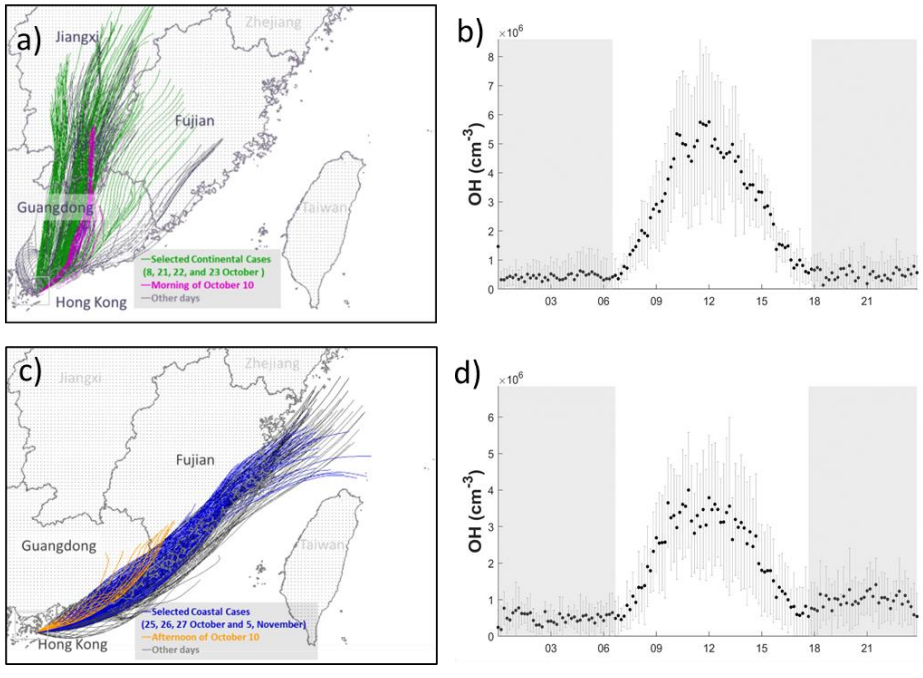

Figure 6. 24 h back trajectories of the continental (a) and coastal (c) cases over the whole measurement period. The selected days for coastal, continental, and mixed cases are labelled in different colours. (b)

https://doi.org/10.5194/egusphere-2022-854
Preprint. Discussion started: 27 September 2022

and (d) show the average concentration of OH with standard deviation in continental and coastal air masses, respectively.

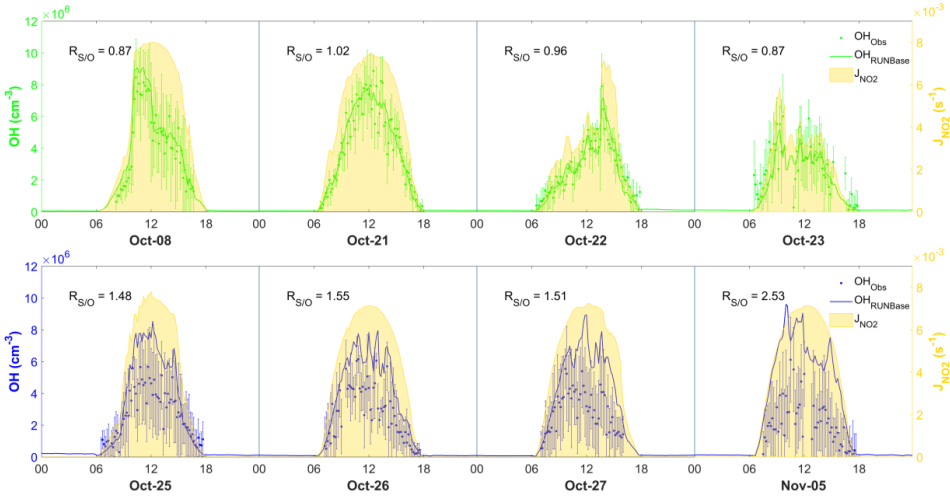

Figure 7. Comparison between observed (dots) and simulated (lines) OH in the four continental cases (top panel) and the four coastal cases (lower panel), also showing measurement uncertainty (error bars) and J_{NO2} measurement (yellow shades).

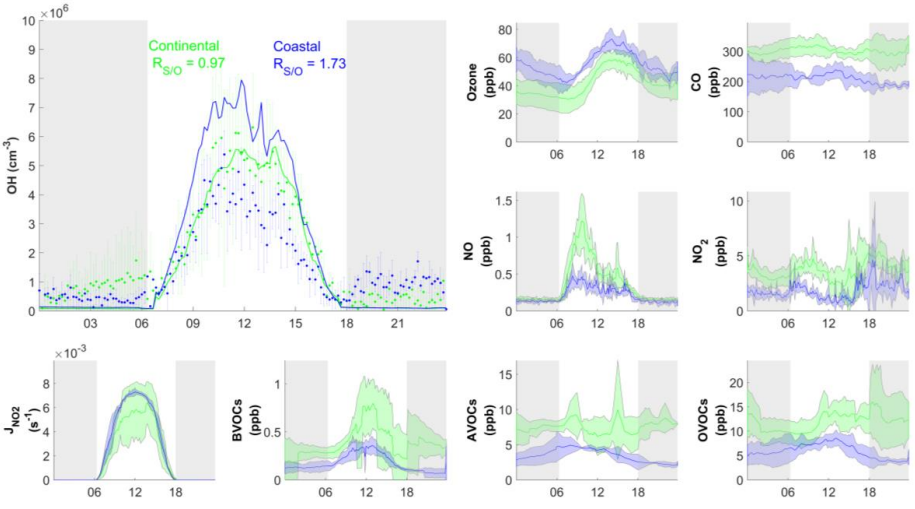

Figure 8. Diurnal profiles of average (± 1σ) concentrations of measured (dots) and simulated (RUNBase, line) OH concentration and important trace gases for selected cases in continental (green) and coastal (blue) air masses. The grey shaded area denotes nighttime.

https://doi.org/10.5194/egusphere-2022-854
Preprint. Discussion started: 27 September 2022

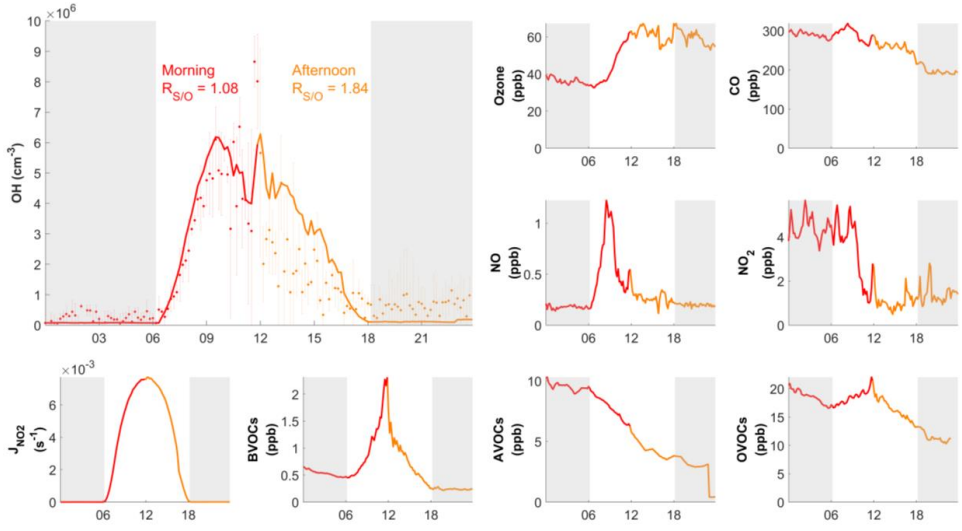

Figure 9. Diurnal profiles of measured (dots) and simulated (RUNBase, line) OH on 10 October 2020, with other chemical species. The air mass drifted from continental (red) in the morning to coastal (orange) in the afternoon. The grey shaded area denotes nighttime.

https://doi.org/10.5194/egusphere-2022-854
Preprint. Discussion started: 27 September 2022

Table 4. OH budgets for the selected continental and coastal cases, morning and afternoon of 10 October.

Continental cases		Coastal cases		10 October (morning)		10 October (afternoon)	
Production							
$HO_2 + NO$	77.57%	$HO_2 + NO$	63.87%	$HO_2 + NO$	70.88%	$HO_2 + NO$	53.73%
HONO + hv	10.09%	HONO + hv	15.01%	HONO + hv	12.19%	HONO + hv	14.14%
O^1D	4.82%	O^1D	10.14%	O^1D	8.39%	O^1D	13.68%
$HO_2 + O_3$	1.79%	$HO_2 + O_3$	4.32%	$HO_2 + O_3$	1.94%	$HO_2 + O_3$	5.65%
CH_3CCH_3OOC	1.25%	CH_3CCH_3OOB	1.22%	$H_2O_2 + hv$	0.68%	$H_2O_2 + hv$	2.56%
Other	4.49%	Other	5.43%	Other	5.93%	Other	10.23%
Loss							
CO	20.04%	CO	22.75%	C_5H_8	15.98%	CO	15.40%
NO_2	9.81%	C_5H_8	7.64%	CO	13.82%	C_5H_8	12.92%
C_5H_8	8.77%	C_2H_5CHO	7.29%	C_2H_5CHO	8.56%	C_2H_5CHO	10.96%
C_2H_5CHO	7.91%	NO_2	7.20%	CH_3CHO	8.51%	CH_3CHO	7.31%
CH_3CHO	7.73%	CH_3CHO	6.79%	NO_2	6.00%	CH_4	3.50%
CH_4	3.68%	CH_4	5.77%	HCHO	3.08%	HCHO	3.49%
HCHO	2.76%	HCHO	2.45%	CH_4	2.73%	NO_2	2.75%
O_3	1.38%	O_3	1.99%	ACR	1.63%	ACR	1.69%
H_2	1.26%	H_2	1.67%	$HOCH_2CHO$	1.42%	$HOCH_2CHO$	1.51%
Other	36.67%	Other	36.45%	Other	38.28%	Other	40.47%

Notes: ACR- acrolein

https://doi.org/10.5194/egusphere-2022-854
Preprint. Discussion started: 27 September 2022

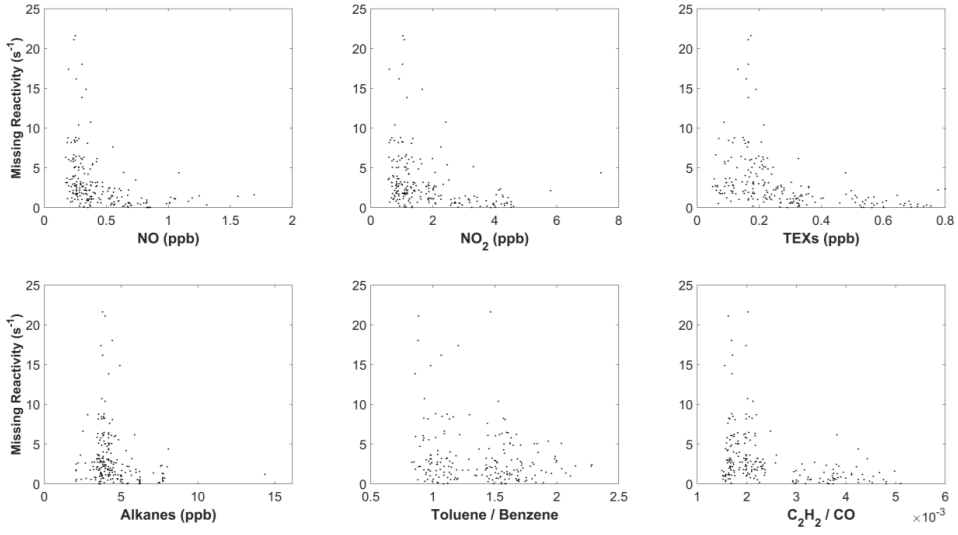

Figure 10. The dependence of calculated missing reactivity on a) NO, b) NO_2, c) TEXs (toluene, ethylbenzene, and xylene), d) alkanes (C_2 to C_8), e) the ratio of toluene to benzene, and f) the ratio of C_2H_2 to CO.